Vol. 641: 79–100, 2020
https://doi.org/10.3354/meps13319

MARINE ECOLOGY PROGRESS SERIES
Mar Ecol Prog Ser

Published May 7

Impact of oysters as top predators on microbial food web dynamics: a modelling approach with parameter optimisation

R. Caillibotte[1,*], Y. Leredde[1], F. Vidussi[2], C. Ulses[3], P. Marsaleix[3], C. Estournel[3], B. Mostajir[2]

[1]Laboratoire Géosciences Montpellier (GM), UMR 5243, CNRS/Université de Montpellier/Université des Antilles, 34090 Montpellier, France

[2]Center of Marine Biodiversity, Exploitation and Conservation (MARBEC), UMR 9190, CNRS/Université de Montpellier/IRD/IFREMER, 34095 Montpellier, France

[3]Laboratoire d'Aérologie (LA), UMR 5560, Université de Toulouse/CNRS/Université Paul Sabatier, 31400 Toulouse, France

ABSTRACT: Aquaculture is becoming a relevant and productive source of seafood, and production is expected to double in the near future. However, bivalve activities can significantly impact coastal ecosystem functioning. To study the direct and indirect impacts of oysters on the microbial food web, a 0D biogeochemical modelling approach was adopted. The model was adjusted by parameter optimisation, assimilating data from several mesocosm observations of concentrations of nitrate, phosphate, silicate, dissolved organic carbon, chlorophyll, and bacterial biomass. The optimisation method provided a set of optimal parameters to fit the experimental observations of 'control' (i.e. natural water without oysters) and 'oyster' (i.e. natural water with oysters) mesocosms. The modelling results showed good accordance with the experimental observations, suggesting that the oysters directly reduced phytoplankton community biomass, thus constraining the ecosystem to a more heterotrophic state. Oysters also reduced competition between bacteria and phytoplankton for nutrient uptake, favouring higher bacterial biomass than in the control experiment. Additionally, the presence of oysters strongly increased large micro-zooplankton biomass (50–200 µm; mainly ciliates and large flagellates). This was a consequence of bacterivory by small zooplankton (5–50 µm; mostly flagellates and small ciliates), providing a trophic link between bacteria and larger zooplankton. In conclusion, parameter optimisation showed good capacity to manage experimental data in order to build a more realistic model. Such models, in connection with future developments in aquaculture and global change scenarios, could be a promising tool for exploited ecosystem management and testing different environmental scenarios.

KEY WORDS: Oysters · Microbial food web · Biogeochemical modelling · Parameter optimisation · Bacteria · Phytoplankton · Zooplankton · Mesocosm

1. INTRODUCTION

Bivalve activities exert a non-neutral influence on coastal ecosystems (e.g. Dupuy et al. 1999, 2000, Chapelle et al. 2000, Mostajir et al. 2015), and an increase in the number of shellfish farms in specific areas will certainly impact nearby ecosystems. The roles of bivalves can be summarised by 3 main functions (Richard et al. 2019): filtration (Dupuy et al. 2000, Trottet et al. 2008), excretion (Mazouni 2004, Richard et al. 2007, Jansen et al. 2011), and biodeposition (Callier et al. 2006, 2009, Robert et al. 2013).

*Corresponding author: remi.caillibotte@gm.univ-montp2.fr

Filtration by oysters selectively removes suspended living or non-living particles from the water column (Gosling 2015, Bayne 2017). Several studies have considered the type and size of particles trapped by oysters, ranging from 3–5 µm (Barillé et al. 1993, Dupuy et al. 1999, 2000) to 500 µm (Barillé et al. 1993, Dupuy et al. 2000, Gosling 2015 and references therein), including nano- (3–20 µm) and microplankton (20–200 µm), comprising phyto-, protozoo-, and metazooplankton. Oyster biodeposition, resulting from the production of faeces and pseudofaeces (Haven & Morales-Alamo 1966), can also influence the ecosystem as it affects the composition of total particulate matter and nutrient recycling. Souchu et al. (2001), comparing suspended particulate matter and dissolved nutrient distributions between oyster farms and nearby areas not used for cultivation in a Mediterranean lagoon (Thau, France), showed that nitrogen (N) in the biodeposits, which accumulated at the water–sediment interface, was recycled by mineralisation to ammonium (NH_4^+), stimulating phytoplankton biomass as a result.

In exploited areas, bivalves can modify microbial plankton community structure (e.g. Froján et al. 2014, Mostajir et al. 2015). For example, a mesocosm study was conducted in the northwestern (NW) Mediterranean lagoon of Thau (France) to assess the structural and functional impacts of oysters on the microbial food web (MFW) (Mostajir et al. 2015). In this confined environment, the authors analysed the autotroph:heterotroph (A:H) carbon (C) biomass ratio structural index, indicating that the MFW became more heterotrophic in the presence of oysters as top predators.

Several modelling studies have simulated the evolution of oysters or their influence on biogeochemical cycles and other MFW components. Two main categories can be distinguished with diverse approaches and goals. The first category of models is focused on oyster evolution and behaviours in a specified environment, comprising models using the dynamic energy budget (DEB) theory (Kooijman 1986, 2000, 2009) and other population growth models (e.g. Gangnery et al. 2001, 2003, 2004). The second category includes models commonly used to investigate bivalve–environment interactions, but where bivalves are considered a forcing factor for the ecosystem. This category concerns biogeochemical models integrating oysters, where biogeochemical models describe MFW processes generally forced by the physical environment (e.g. temperature and light). Several studies have included the N and/or phosphorus (P) cycles (e.g. Chapelle et al. 2000, Zaldívar et al. 2003). In parallel with these developments and because of the strong coupling between physics and biology, biogeochemical models are regularly coupled with 3-dimensional (3D) oceanic circulation models (e.g. Auger et al. 2014, Plus et al. 2015, Ulses et al. 2016). Other developments have been made in coupling biogeochemical models including bivalves with hydrodynamic models to simulate food availability and thus the carrying capacities of bivalve populations (Duarte et al. 2003, Marinov et al. 2007) or the impact of bivalves on the spatial distribution of phytoplankton (Spillman et al. 2008, Cugier et al. 2010, Ibarra et al. 2014).

The present study focused on the interaction between oysters and MFW components and fluxes, using a 0D modelling approach. This work was part of the development of a 3D coupled hydrodynamic–biogeochemical model of an exploited coastal NW Mediterranean lagoon (Thau, France). The Thau lagoon is a shallow marine lagoon connected to the sea by 3 narrow channels. It has been highly exploited for bivalve culture and, in particular, the culture of the non-native oyster *Crassostrea gigas*, which has been cultivated in the lagoon since 1972 (Hamon et al. 2003). The originality of the present study lies in the insertion of a new oyster compartment into the highly comprehensive Eco3m-S biogeochemical model, presented in detail in Auger et al. (2011), forming part of the development of a coupled model of the exploited Thau lagoon. An optimisation method assimilating mesocosm observations described in Mostajir et al. (2015) was performed to determine the best control parameters for the model. The Eco3m-S biogeochemical model was used to simulate complex ecosystem dynamics composed of several cycles of biogenic elements (C, N, P, and silica, Si). The new oyster compartment was implemented to investigate the impact of the insertion of oysters as top predators of the MFW. The mesocosm study of Mostajir et al. (2015) showed very good experimental results regarding MFW structure and functioning resulting from the introduction of oysters, but some questions remained unsolved. The advantage of the new model is that it provides high-frequency results and deeper insight into interactions and fluxes within the MFW. In further studies, the model could also be used to elucidate the potential response of the ecological system to new environmental conditions and forcings. Future studies involving this new model will use 3D coupled hydrodynamic–biogeochemical modelling of the same study area. Specific questions addressed by the current study were (1) What are the essential

biogeochemical processes modified within the MFW by the insertion of oysters? (2) What are the direct and indirect impacts of the insertion of oysters on the different components of the MFW?

2. MATERIALS AND METHODS

2.1. Experimental data

A mesocosm study was conducted at the Mediterranean Centre for Marine Ecosystem Experimental Research (MEDIMEER) (Mostajir et al. 2015) based at the marine station of Sète (southern France). The purpose was to determine the MFW structural and functional responses to oysters as top predators. Four mesocosms filled simultaneously with screened (<1000 µm) natural Thau lagoon surface water were studied over 10 d in October 2005 near the MEDIMEER pontoon. Two of the mesocosms contained only natural water ('Control'), and 2 contained 10 *Crassostrea gigas* each ('Oyster'). These mesocosms mimicked a water column without including a sedimentary compartment. Water-column homogeneity was maintained with a mixing pump.

The present modelling study does not reproduce all observations described in Mostajir et al. (2015) because only a few of them were relevant for the model. Temperature and photosynthetically active radiation (PAR: 400–700 nm) were used as external forcings. In total, 6 experimental observations, detailed below, were used to initialise the numerical model on Day 0 (beginning of the mesocosm experiment) and for parameter optimisation thereafter.

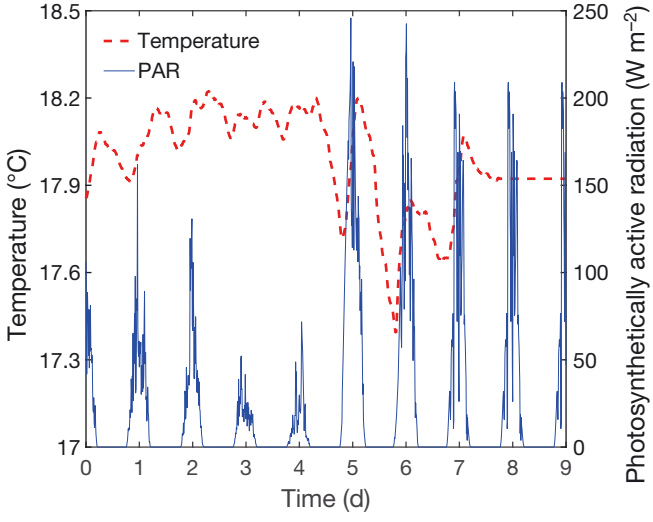

Fig. 1. Temperature and photosynthetically active radiation (PAR) measured in the Thau lagoon (southern France) during the experimental mesocosm study and used to force the biogeochemical model

Temperature (Fig. 1) was measured every 10 min throughout the mesocosm experiment. PAR (Fig. 1) was recorded every 10 min, between 14:00 h on Day 0 and 23:50 h on Day 7. On Day 8, measurements were stopped due to sensor failure; however, to complete our model's forcings, the observed values obtained on Day 7 were replicated on Days 8 and 9. Nutrient concentration data (nitrate [NO_3^-]: Figs. 2A & 3A; phosphate [PO_4^{3-}]: Figs. 2B & 3B; silicate [SiO_4^{2-}]: Figs. 2C & 3C) as well as dissolved organic carbon (DOC) concentration data (Figs. 2D & 3D) were determined with samples taken once a day at 10:00 h from Day 1 until Day 9. Chlorophyll *a* (chl *a*) concentration (Figs. 2E & 3E) was measured using high-performance liquid chromatography (HPLC). Bacterial abundances measured by flow cytometry were converted to C biomass (in mmol of C m^{-3}; Figs. 2F & 3F) using a factor of 20 fg C bacterium^{-1} (Sime-Ngando et al. 1995, Vidussi et al. 2011). More details about the experimental observations can be found in Mostajir et al. (2015).

2.2. Model description and initial simulation

The Eco3m-S biogeochemical model used in this study is presented in detail in Auger et al. (2011). It was built to simulate the temporal evolution of a complex ecosystem composed of several decoupled cycles of biogenic elements (C, N, P, and Si), with a mechanistic approach for biogeochemical processes. A schematic view of the model is presented in Fig. 4. The Eco3m-S model includes 36 variables, comprising photoautotroph and heterotroph biomasses, non-living particulate organic matter (POM) concentration, dissolved organic matter (DOM) concentration, and nutrient and oxygen concentrations (detailed in Table 1). The initial model comprises 166 fundamental control parameters defining the modelled biogeochemical processes. As an example, the model requires 10 parameters to define the grazing function of the first zooplankton size class (5–50 µm).

The model is composed of several plankton groups characterised by their functional type, resulting from an analysis of experimental and modelling information on the biogeochemical functioning of the NW Mediterranean Sea. Autotrophs included 3 size classes of phytoplankton: 0.7–2 µm (Phy_1), >2–20 µm (Phy_2), and >20–200 µm (Phy_3; largely dominated by silicifiers such as diatoms); heterotrophs included 4 size

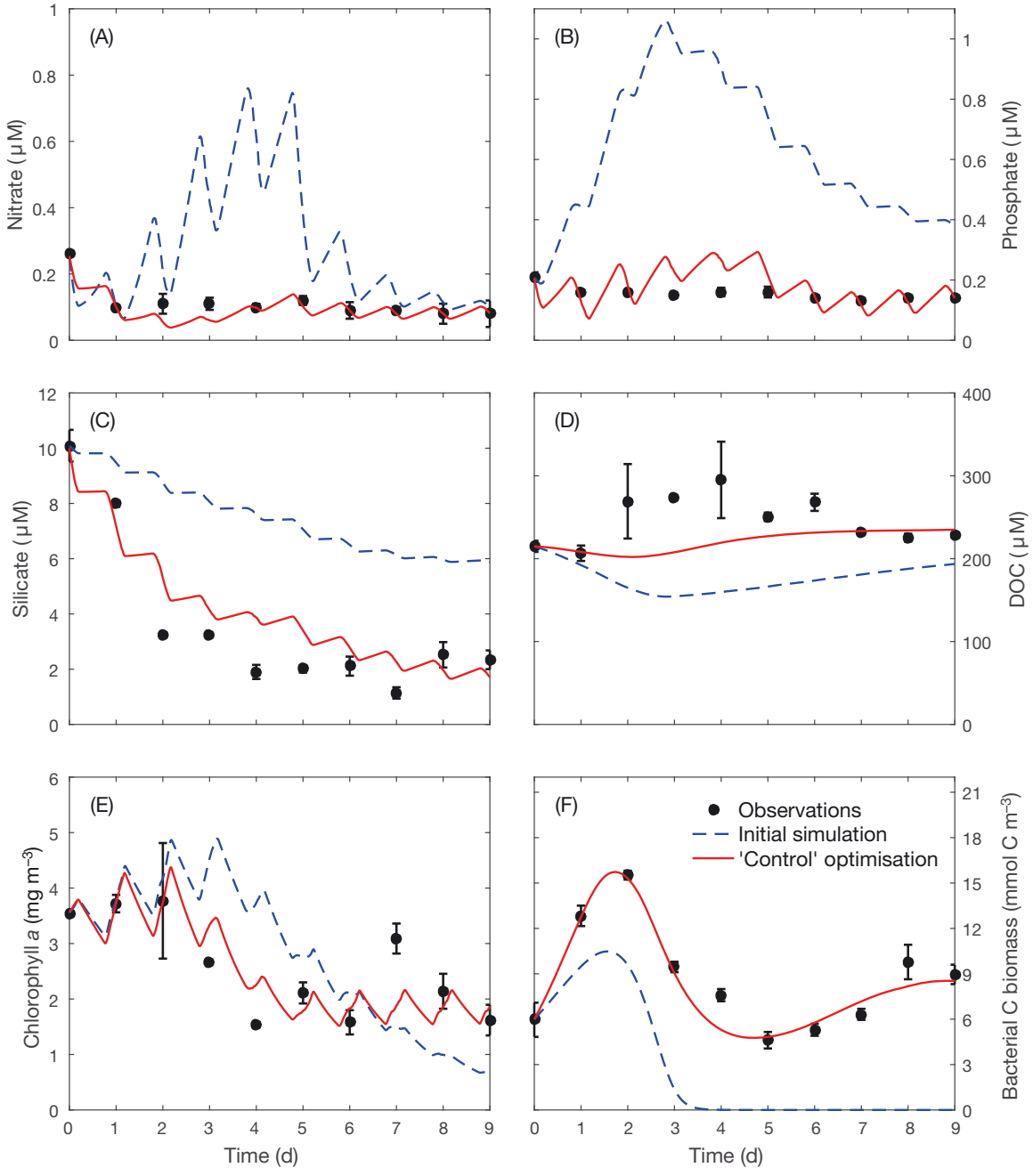

Fig. 2. Concentrations of (A) nitrate, (B) phosphate, (C) silicate, (D) dissolved organic carbon (DOC), (E) chlorophyll *a*, and (F) bacterial C biomass from the mesocosm experimental observations (means, with whiskers showing range, n = 2), and the modelled (Control) initial simulation and Control optimisation

classes: 0.3–1 µm (Bact; mainly bacteria), 5–50 µm (Zoo_1; mostly bacterivorous flagellates and small ciliates), >50–200 µm (Zoo_2; mainly ciliates and large flagellates), and >200 µm (Zoo_3; metazooplankton dominated by copepods). To ease the comparison with the total chl *a* concentration measurements, only one group of phytoplankton (Phy) was considered in our study, representing the entire phytoplankton community. The initial parameters of this group were similar to the parameter values of Phy_3, because diatoms dominated the phytoplankton community during the mesocosm experiment. Optimal parameters obtained by our method thus correspond to the total phytoplankton community. However, the 3 types of zooplankton were maintained in the model, as they prey on different groups of living

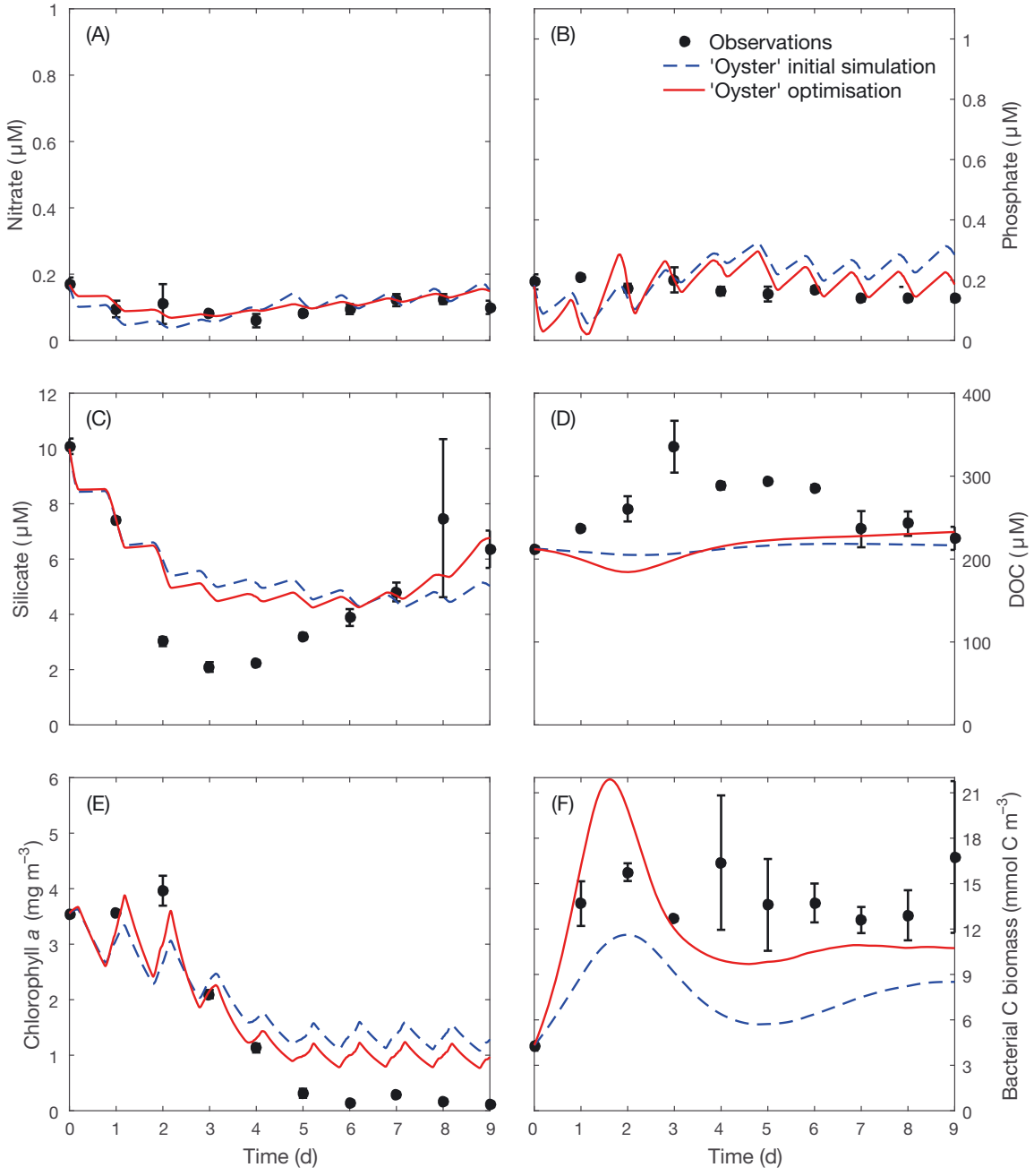

Fig. 3. Concentrations of (A) nitrate, (B) phosphate, (C) silicate, (D) dissolved organic carbon (DOC), (E) chlorophyll *a*, and (F) bacterial C biomass from the mesocosm experimental study observations (means, with whiskers showing range, n = 2), and the modelled Oyster initial simulation and Oyster optimisation

organisms (bacteria, phytoplankton, and even smaller zooplankton) or non-living POM (see Fig. 4).

Four types of dissolved inorganic nutrients were considered: NO_3^-, NH_4^+, PO_4^{3-}, and SiO_4^{2-}. The distinct roles of NO_3^- and NH_4^+, which are involved in new and regenerated production, were taken into account. DOM (in the forms of C, N and P) was also considered, as it was consumed by heterotrophic bacteria. Non-living POM (in the form of C, N, P, and Si) was divided into 2 size classes: ≤50 µm (light) and >50 µm (heavy). Light non-living POM was also in the form of chlorophyll, resulting from phytoplankton death and zooplankton egestion.

Experimental observations of nutrients, DOC, bacteria and chl *a* on Day 0 fixed some of the initial conditions required for running the model. Without

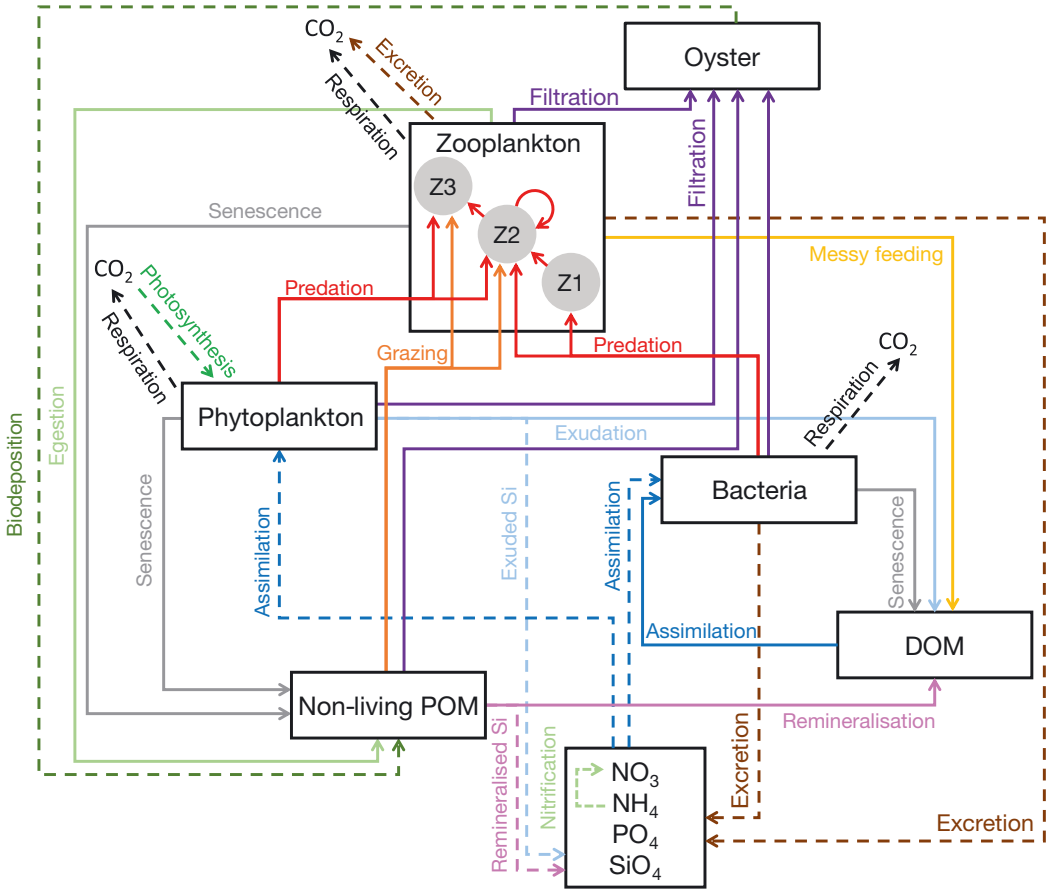

Fig. 4. The ecosystem model showing the main functional groups, biochemical constituents and processes, adapted from Auger et al. (2011). A new compartment for oysters was introduced, filtering particulate matter from the water column. Within the zooplankton box, 3 functional groups were considered (Z1, Z2, Z3), preying selectively upon other zooplankton groups, phytoplankton, bacteria, and non-living particulate organic matter (POM). DOM: dissolved organic matter

Table 1. List of state variables in the Eco3m-S model. Zooplankton — Zoo_1: 5–50 µm (mostly bacterivorous flagellates and small ciliates); Zoo_2: >50–200 µm (mainly ciliates and large flagellates); Zoo_3: >200 µm (metazooplankton dominated by copepods)

State variables	Description	Units
NO_3^-, NH_4^+, PO_4^{3-}, SiO_4^{2-}	Nitrate, ammonium, phosphate, silicate	mmol m^{-3}
X_{Phy}	Phytoplankton community in X, where X corresponds to carbon (C), nitrogen (N), phosphorus (P), or silica (Si)	mmol X m^{-3}
Chl_{Phy}	Phytoplankton in chlorophyll	mg chl m^{-3}
C_{Zoo_1}, C_{Zoo_2}, C_{Zoo_3}	Zooplankton C biomass	mmol C m^{-3}
C_{Bact}	Bacterial C biomass	mmol C m^{-3}
DO_X	Dissolved organic X, with X = C, N, P, or Si	mmol X m^{-3}
nl-POX_y	Heavy (y = h) and light (y = l) non-living particulate organic X (organic detritus), with X = C, N, P, or Si	mmol X m^{-3}
Chl_{Det}	Light chlorophyll detritus coming from phytoplankton death or egestion of zooplankton	mg chl m^{-3}

any information on non-living matter, initial non-living POM concentrations were set to zero at the beginning of the experiment. Since the experimental study did not provide zooplankton biomasses, the initial conditions for Zoo_1, Zoo_2, and Zoo_3 were fixed after calibration. The water column was considered to be well-mixed, so the oxygen concentration was set to be sufficient (200 mmol m^{-3}) to avoid limiting biogeochemical processes. Temperature and PAR measured during the mesocosm experiment were used in the model to force biogeochemical processes.

Once initial conditions were established and forcings were defined, an initial simulation was performed to simulate the 10 d of the experiment, using parameters suitable for the NW Mediterranean Sea where the model is usually implemented (Auger et al. 2011). The model can provide daily variations in the 36 variables at a high frequency, typically every 10 min, for applied simulations. In fact, this interval of time corresponds to the time step chosen to resolve the differential equations of the model. Biogeochemical fluxes such as primary production, grazing, and respiration were extracted as outputs of the model.

The results obtained for this initial simulation were then compared with the available data (NO_3^-: Fig. 2A; PO_4^{3-}: Fig. 2B; SiO_4^{2-}: Fig. 2C; DOC: Fig. 2D; chl *a*: Fig. 2E; bacteria: Fig. 2F). The model results provided the same orders of magnitude as the experimental data, even though the 2 sets of magnitudes did not exhibit similar patterns. For instance, the N, P, and Si nutrient concentrations were excessively high. However, N concentrations were similar to the experimental data at the end of the experiment. It should also be noted that bacterial C biomass was reduced to zero after Day 4 of the experiment. Because bacteria were involved in the decomposition process and assimilation of DOM, the very low simulated bacterial biomass led to discrepancies between model results and experimental data in terms of nutrients and DOM. The model also provided additional information such as NH_4^+ concentration (see Fig. 5A) and zooplankton biomasses (see Fig. 5B) for which no corresponding experimental data were measured.

2.3. Optimisation method

To reduce discrepancies between experimental observations and biogeochemical model results, an optimisation method suggested by Prunet et al. (1996) was adopted. The mathematical method is described through Eqs. (A1) to (A8) in Appendix 1. The mesocosm experiment provided a total of 54 experimental observations by the measurement of 6 variables, once a day, for 9 d (see Section 2.1; Day 0 was used as the initial condition). The aim of this mathematical method was to modify and optimise the biogeochemical control parameters of the model in order to minimise a cost function representing the gap between observations and model results.

The value of the cost function was used to determine if the model results became more similar to the experimental observations with the iterative optimisation method. In the present study, for the first iteration, the control parameter values were extracted from the literature (see Auger et al. 2011) and corresponded to the initial simulation.

The optimisation method was used to assess the parameter resolutions, which were estimators of the determination of each control parameter. Similar information concerning the data was assessed, i.e. data resolutions showing the contribution of each observation as useful information the optimisation method (e.g. Wunsch 1978).

The optimisation procedure involved all 166 parameters; however, in practice, most of them had a weak influence on the results. For example, as noted above (Section 2.2), the oxygen concentration was sufficient to avoid limiting biogeochemical processes. Thus, the modification of parameters linked with oxygen processes did not affect our results, and the resolutions of these parameters were always null.

2.4. System of equations for oysters

To insert the new compartment for oysters into the ecosystem model, a method inspired by Chapelle et al. (2000) was applied, assuming 2 main functions. The first function was the filtration of all living (zooplankton, phytoplankton, and bacteria) and non-living (non-living POM) particles. The second function was biodeposition (e.g. pseudofaeces). These 2 processes defined the temporal evolution of oyster biomass ($[Oyster]_C$), expressed as C concentration (mmol C m^{-3}):

$$\frac{d[Oyster]_C}{dt} = \sum filt_X - biodO \quad (9)$$

where $filt_X$ is the filtration by oysters of the living and non-living particulate matter X present in the water column (bacteria, Zoo_1, Zoo_2, Zoo_3, Phy, and light and heavy non-living POM). Bacteria were also considered in the filtration process as they can be attached to larger non-living particulate matter (Frikha et al. 1987, found in De Crignis 2007), but the efficiency of this filtration was assumed to be very low (see Table 2). The biodO term corresponds to the biodeposition of non-living POM (light and heavy). The first modelling results showed no impact of oyster excretion on the water column for this specific experimental period. Therefore, this process was not modelled in this study to reduce the number of control parameters needed and simplify the optimisation method. However, this process certainly needs more experimental data and modelling efforts, as it may affect the MFW over time periods longer than the 10 d of the present

mesocosm experiment. The variables and fluxes presented here were first calculated in units of C, as were the processes in other compartments. To include filtration efficiency, $effO_X$, for each filtered particle X, the filtration term was expressed as in Eq. (10):

$$filt_X = \alpha_{filt} \times effO_X \times [X]_C \quad (10)$$

The coefficient α_{filt} depends on temperature, oyster biomass, and the maximum filtration rate of oysters ($filt_0$):

$$\alpha_{filt} = filt_0 \times f(T) \times [Oyster]_C \quad (11)$$

where, in addition to other temperature-dependent processes, f(T) represents the temperature limitation of the biological process. This variable was expressed with the commonly used Q_{10} model (e.g. Sherman et al. 2016):

$$f(T) = Q_{10}^{(T_{ref}-T)/10} \quad (12)$$

The biodO term was calculated as a constant fraction of predation (bd%; Mazouni 1995, Chapelle et al. 2000):

$$biodO = bd_{\%} \times \sum filt_X \quad (13)$$

To impact other compartments of the biogeochemical model, the filtration term was included as a sink term for each filtered particle, and the biodeposition term was included as a source term for light and heavy non-living POM. A total of 14 new parameters (Table 2) were introduced to the existing Eco3m-S model in order to control the 2 main functions of oysters.

3. RESULTS

The results of this study are presented in 2 parts. The first part provides the results of the 'Control' optimisation (corresponding to the results of the optimisation procedure applied for the initial Eco3m-S model, before the addition of the new oyster compartment). The second part presents the results of the 'Oyster' optimisation, corresponding to the new biogeochemical model including oysters. Each part is discussed in 3 steps: a description of simulation results, an analysis of adjusted parameters, and an analysis of data resolutions.

3.1. Control optimisation

The optimisation method was first performed on the original biogeochemical model, without the oyster compartment, using the experimental observations available for the Control mesocosms (i.e. including the entire MFW but without oysters). The initial simulation presented in Section 2.2 was used as the first guess. Similar weights for the observations were imposed (managed by matrix W; see the Appendix). The optimisation sequence, aiming at minimising the cost function and optimising the parameters of the model, was iterated 47 times (i.e. 47 × 167 simulation runs) until the parameters reached a fixed value and plateaued. The value of the cost function ranged from 1.00 initially to 0.08 at the end.

Table 2. New parameters for oysters introduced to the Eco3m-S model. (1) Chapelle et al. (2000), (2) Le Gall et al. (1997), (3) Defossez & Hawkins (1997), (4) De Crignis (2007) (5) Dupuy et al. (2000), (6) Grant et al. (2008), (7) Mazouni (1995), (8) Le Gall & Raillard (1988). Zoo: zooplankton; Phy: phytoplankton; POM: particulate organic matter. Parameters are unitless except maximal filtration rate (s^{-1}) and reference temperature for oysters (°C)

Name		Initial value	Final value	Resolution
Maximal filtration rate[1]	$filt_0$	2.31×10^{-7}	2.02×10^{-7}	0.05
Filtration efficiency on Zoo_3	$effO_{Zoo3}$	0.00	0.00	0.00
Filtration efficiency on Zoo_2[2,3,4,5]	$effO_{Zoo2}$	0.10	0.10	0.00
Filtration efficiency on Zoo_1[2,3,4,5]	$effO_{Zoo1}$	0.15	0.15	0.00
Filtration efficiency on Phy_3[2,4,5]	$effO_{Phy3}$	0.50	0.45	0.02
Filtration efficiency on Phy_2	$effO_{Phy2}$	0.00	0.00	0.00
Filtration efficiency on Phy_1	$effO_{Phy1}$	0.00	0.00	0.00
Filtration efficiency on bacteria[2,4]	$effO_{Bact}$	0.05	0.05	0.00
Filtration efficiency on light non-living POM[2,6]	$effO_{lDet}$	0.10	0.10	0.00
Filtration efficiency on heavy non-living POM[2,6]	$effO_{hDet}$	0.10	0.10	0.00
Biodeposition rate[7]	$bd_{\%}$	0.30	0.34	0.02
Fraction of light non-living POM in biodeposits (with the rest being heavy)	k_{Det}	0.50	0.48	0.01
Temperature coefficient for the oyster temperature function[1]	Q_{10}^{oyster}	2.00	2.02	0.00
Reference temperature for oysters[1,8]	T_{ref}^{oyster}	18.00	21.07	0.08

The Control optimisation was thus more similar to the experimental observations than the initial simulation was.

3.1.1. Simulation results

Nutrient concentrations for the Control optimisation were more similar to the experimental observations than were the initial simulation results. For NO_3^- concentration (Fig. 2A), the gap between the Control optimisation results and observations was 0.03 µM on average, whereas the gap was 0.1 µM for the initial simulation. The amplitude of daily variations was also reduced by the optimisation procedure. Between Days 3 and 4, the concentration ranged from 0.05–0.10 µM, whereas it was 0.33–0.76 µM in the initial simulation.

Concerning PO_4^{3-} concentration (Fig. 2B), from the beginning until Day 3, the decrease in PO_4^{3-} during the daytime was greater in the Control optimisation than in the initial simulation. However, the increase in PO_4^{3-} concentration at night was lower for the optimised simulation. The mean concentration over the entire period was 0.18 µM for the optimised simulation, compared to 0.16 µM for the experimental observations.

The SiO_4^{2-} concentration (Fig. 2C) for the Control optimisation was lower than that for the initial simulation. The values obtained remained generally larger than the observations, but the trend was well represented. The optimised average concentration throughout the study period was 4.04 µM, compared to 7.50 µM in the initial simulation.

The NH_4^+ concentration (Fig. 5A) increased gradually from Day 0 (0.3 µM) until Day 5 (3.2 µM) in the Control optimisation. Thereafter, it was stable around a value of 2.6 µM, in contrast to the initial simulation, in which the concentration decreased towards a much lower value (i.e. 0.3 µM at the end of the initial simulation).

The DOC concentration (Fig. 2D) in the optimised simulation decreased less than that in the initial simulation and was nearly constant throughout the experimental period. It ranged from 202–235 µM. The maximum experimental values of DOC observed during Days 3 and 4 were not captured by the optimised simulation.

Regarding the chl *a* concentration (Fig. 2E) for the optimised simulation, the results were more similar to the observations than were those obtained with the initial simulation. The simulated results followed the behaviour of measurements taken during the mesocosm experiment. The decrease in chl *a* concentration on Day 3 was corrected by the optimisation procedure to fit the experimental points. From Day 5 until the end, the amplitude of the daily variations was almost constant for the Control optimisation, with an increase during daytime equal to the decrease during night-time (approximately 0.6 mg m^{-3}). Hence, the simulation did not reproduce the experimental observations on Day 7 but was clearly consistent with the last few days.

The most significant improvement was in the bacterial C biomass concentration (Fig. 2F), which showed a good fit of the control optimisation with experimen-

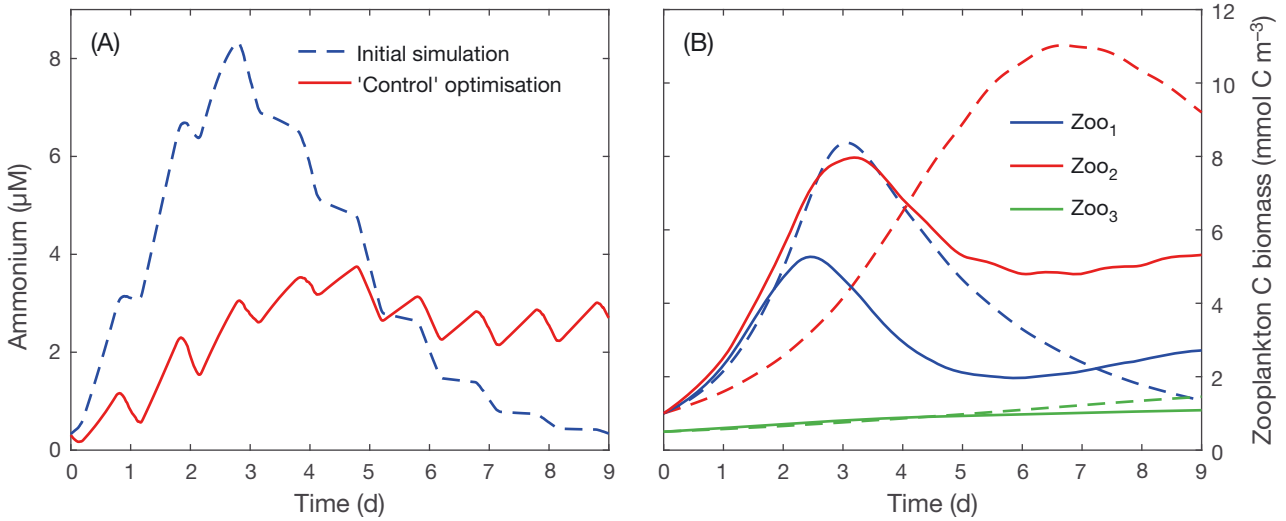

Fig. 5. Comparison between the initial simulation (dashed lines) and Control optimisation (solid lines) for concentrations of (A) ammonium and (B) zooplankton C biomass. In (B), the 3 compartments of zooplankton are represented: Zoo_1 (blue; mostly bacterivorous flagellates and small ciliates), Zoo_2 (red; mainly ciliates and large flagellates), and Zoo_3 (green; metazooplankton dominated by copepods)

tal observations. In contrast to the initial simulation, the values obtained were not reduced to zero after Day 4. Note that bacterial growth during the first few days was higher in the optimised simulation than in the initial simulation. The concentration reached a maximum of 15.73 mmol C m^{-3} on Day 2 and a minimum of 4.76 mmol C m^{-3} between Days 4 and 5, compared to 15.52 and 4.61 mmol C m^{-3} for the observations, respectively.

Zoo_1 and Zoo_2 C biomass concentrations (Fig. 5B) in the Control optimisation followed a similar increase for the first 2 d of the experiment, contrary to those in the initial simulation. Then, the Zoo_2 C biomass concentration exceeded the Zoo_1 concentration, which depicted a link of predation. Between Days 2 and 3, the 2 concentrations reached a maximum (5.26 and 7.97 mmol C m^{-3} for Zoo_1 and Zoo_2, respectively). From Day 3 until the end of the experiment, Zoo_1 and Zoo_2 showed similar patterns, and the gap between the 2 concentrations remained almost constant. At the end, the Zoo_1 and Zoo_2 concentrations were 2.72 and 5.32 mmol C m^{-3}, respectively. The C biomass concentration of Zoo_3 was almost the same in the Control optimisation and the initial simulation.

3.1.2. Analysis of adjusted parameters

The method used in this study estimated the resolution of each parameter, i.e. the importance of each parameter for making the simulated results more similar to the observations. Parameter resolution was used to sort parameters and identify the key parameters for the optimisation procedure (Table 3). A small change in these parameters can affect the whole biogeochemical simulation. Therefore, modification of these key parameters by the optimisation procedure was investigated. Table 3 presents a list of key parameters presenting both a high resolution rate and a significant change.

Seven parameters among the identified key parameters (Table 3) controlled the zooplankton processes. The preference factor of micro-zooplankton for nano-zooplankton and the maximum grazing rate of micro-zooplankton both increased in the process, with changes of +64 and +86%, respectively. This led to higher predation of Zoo_1 by Zoo_2 in the Control simulation compared to that in the initial simulation. This might explain the shifting in time of the maximum Zoo_2 C biomass concentration (Fig. 5B), happening on Day 7 in the initial simulation and on Day 3 in the Control simulation. Zoo_2 preys on Zoo_1, and the change in the dynamics of Zoo_2 also impacted the dynamics of Zoo_1, with a diminution of the maximum Zoo_1 C biomass concentration. The maximal grazing rate of nano-zooplankton decrease also participated in this change.

Two of the selected parameters shown in Table 3 correspond to the growth of bacteria. During the optimisation procedure, the net growth efficiency of bacteria greatly increased from 0.3–0.99, whereas the maximum uptake rate of bacteria decreased from 4.25–1.97 × 10^{-5} s^{-1}. In our model, the growth of bacteria depended on the product of these 2 parameters. Finally, this modification led to an increase in total bacterial growth in the Control optimisation compared to the initial simulation (see Fig. 2F). These 2

Table 3. Key parameters that changed during the Control optimisation process assimilating Control mesocosm observations. DOC: dissolved organic carbon; Phy: phytoplankton; Zoo: zooplankton

Name	Initial value	Final value	Units	Resolution
Maximum uptake rate of bacteria for DOC	4.25 × 10^{-5}	1.97 × 10^{-5}	s^{-1}	0.78
Maximal chl:N ratio of Phy	2.30	2.03	mg chl (mmol N)$^{-1}$	0.77
Reference temperature for zooplankton processes	18.00	12.50	°C	0.64
Maximal internal Si:C ratio of Phy	0.19	0.38	mol Si (mol C)$^{-1}$	0.58
Maximal internal N:C quota of Phy	0.20	0.19	mol N (mol C)$^{-1}$	0.54
Preference factor of Zoo_2 for Zoo_1	0.25	0.41	–	0.49
Half-saturation constant for nitrate uptake for Phy	1.00	2.24	mmol N m^{-3}	0.49
Maximal grazing rate of Zoo_1	4.50 × 10^{-5}	3.68 × 10^{-5}	s^{-1}	0.40
Net growth efficiency of zooplankton	0.80	0.75	–	0.38
Maximal grazing rate of Zoo_2	3.00 × 10^{-5}	5.60 × 10^{-5}	s^{-1}	0.37
Net growth efficiency of bacteria	0.30	0.99	–	0.36
Maximal internal P:C quota of Phy	1.90 × 10^{-2}	2.85 × 10^{-2}	mol P (mol C)$^{-1}$	0.34
Preference factor of Zoo_2 for Phy	0.15	0.06	–	0.29
Reference temperature for decomposition processes	20.00	9.37	°C	0.28
Fraction of messy feeding for zooplankton	0.23	0.31	–	0.27
Maximal nitrification rate at 0°C	5.91 × 10^{-7}	2.52 × 10^{-7}	s^{-1}	0.17
Temperature coefficient for decomposition	2.95	4.35	–	0.16

changes are antagonistic and highlight the fact that the optimisation process modified combinations of parameters and not individual parameters.

The decrease in the maximal nitrification rate from 5.91–2.52 × 10^{-5} s^{-1} contributed to the diminution of NO_3^- concentration (Fig. 2A) in the Control optimisation compared to the initial simulation.

The temperature coefficient for decomposition increased from 2.95–4.35°C^{-1}, and the reference temperature for decomposition greatly decreased. This change impacted the decomposition process, which was temperature-dependent in our model. The decomposition process converts, via the action of bacteria, non-living POM into DOM. The modification of these 2 parameters, in addition to higher bacterial C biomass (Fig. 2F), led to an increase in DOC concentration (Fig. 2D). Decomposition and other temperature-dependent processes in the model (primary production of phytoplankton, grazing by zooplankton, nitrification, etc.) were modified by the optimisation procedure by changing the reference temperature and/or the temperature coefficient. These 2 parameters acted as highly non-linear parameters. The adjustment of these 2 parameters is important, as the temperature varied during the experiment period. For example, on Day 5, the temperature variation was approximately 0.8°C (Fig. 1), the temperature function of zooplankton processes, phytoplankton processes, and decomposition was reduced by 8, 6, and 12%, respectively.

The internal quotas for Phy (N:C, P:C, and Si:C ratios) were also changed during the optimisation process. The range of the Si:C ratio increased as the maximal internal ratio was changed from 0.19–0.38 mol Si (mol C)$^{-1}$. The phytoplankton community could thus consume more SiO_4^{2-} to build their skeleton or frustules (in the case of diatoms). From the initial simulation to the Control optimisation, the SiO_4^{2-} concentration (Fig. 2C) decreased, becoming more similar to the observations. The consumption of NO_3^- by the phytoplankton community varied less (see Fig. 2A) because the interval length of the N:C quota, i.e. the gap between the minimum internal N:C and maximal internal N:C quota, was reduced. Similarly, the interval length of the P:C quota increased, allowing more PO_4^{3-} uptake by the phytoplankton community.

Several parameters presented a very large resolution, with a maximum of 0.78, but none of them had a resolution equal to 1. Thus, a change in a single parameter value was not enough to adjust our model. The optimisation procedure modified a linear combination of parameters.

3.1.3. Analysis of data resolution

The optimisation method allowed the calculation of data resolutions, which represent the contribution of each observation as effective information to optimise the model. Fig. 6A shows data resolutions for the Control optimisation, for the last iteration of the optimisation procedure. The data resolution varied between sets of observations, which depended on sampling time. Therefore, the data resolutions also varied during the experimental period.

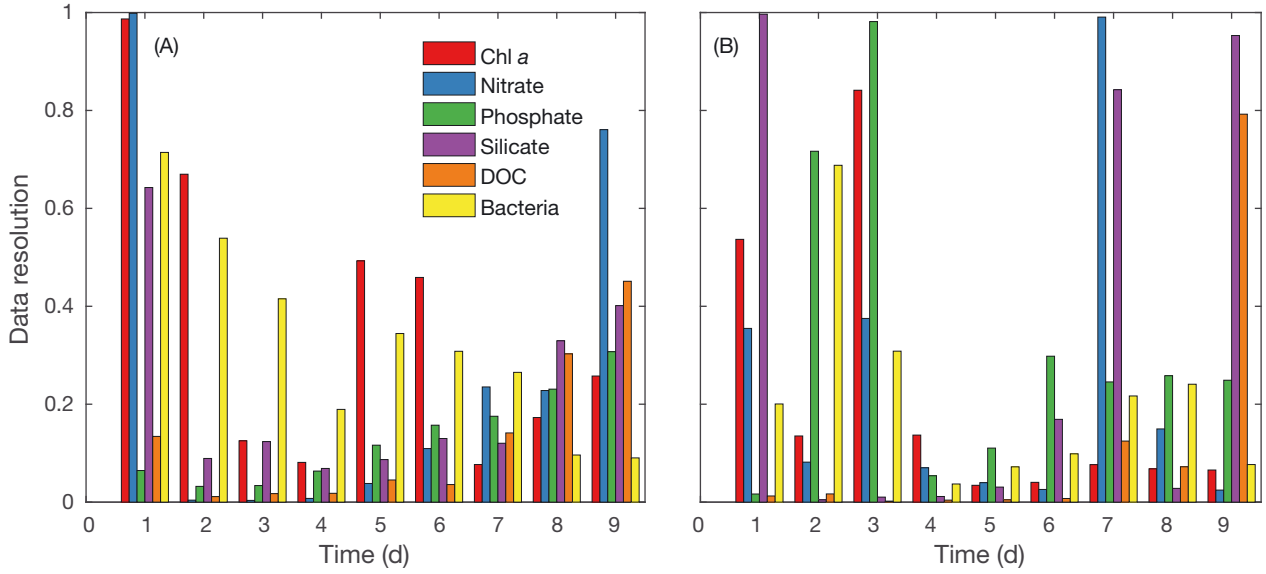

Fig. 6. Data resolution for each type of observation, detailed for each day of the experiment for the (A) Control and (B) Oyster optimisations. DOC: dissolved organic carbon

Experimental observations of the chl *a* concentration were important for the optimisation procedure as they had the highest data resolution among the available observations. The data resolution decreased from 1.00 on Day 1 to 0.08 on Day 4, and then reached 0.49 and 0.46 on Days 5 and 6, respectively. At the end of the period, it remained below 0.25. The NO_3^- data also had a high resolution at the very beginning and during the last few days of the experiment. The resolution of the PO_4^{3-} data increased throughout the experimental period, from 0.06 initially to 0.31 at the end. The resolution of the SiO_4^{2-} data followed the same trend as that of the PO_4^{3-} data, except on Day 1, when the SiO_4^{2-} data were more useful for the optimisation process. The DOC data showed the same increase as the PO_4^{3-} data. However, on Days 2, 3, and 4, the resolution of the DOC data was very low. The resolution of the bacterial data decreased and varied between 0.71 and 0.09 during the experimental period.

On Day 1, the chl *a* and NO_3^- observations presented the highest resolutions for the optimisation process. From Days 2 to 6, the chl *a* and bacterial C biomass observations were the most influential. During those 5 days, the resolution of other observations remained low in comparison, except that of SiO_4^{2-} on Day 3. At the end of the period, the resolutions were almost homogeneous among observations, even if the NO_3^- data had a relatively high resolution.

3.2. Oyster optimisation

To estimate the best parameter values for the model including the new oyster compartment, an optimisation procedure was performed with 180 parameters (166 initially and 14 added for oysters). Realistic values for the new parameters were chosen according to the literature (see Table 2). The initial value of $filt_0$ was set to 2.31×10^{-7} s^{-1}, as suggested by Chapelle et al. (2000), and derived from Mazouni et al. (1996). The biodeposition rate, $bd_{\%}$, was initially set at 0.3 (Mazouni 1995). The coefficients of $effO_X$ were arbitrarily chosen (see Table 2) but were free to change with the optimisation process, as were other parameters. As previously mentioned, only one group of phytoplankton was considered, representing the entire phytoplankton community. However, the model included 3 filtration efficiencies for phytoplankton that can be used with 3 size classes of phytoplankton in future developments; 2 of them were useless for our study and were thus fixed at zero. Experimental observations from mesocosms including oysters as top predators (Mostajir et al. 2015) were assimilated. The first guess of the method included the 166 parameter values resulting from the Control optimisation plus the 14 new parameter values, defined as the Oyster initial simulation. The optimisation process was iterated 75 times (i.e. 75 × 181 simulation runs). The cost function ranged from 1.00 for the Oyster initial simulation to 0.51 for the Oyster optimisation.

3.2.1. Simulation results

The NO_3^- concentration after optimisation was very similar to that in the observations (Fig. 3A). The simulated mean value over the entire period in the Oyster optimisation was 0.108 µM, compared to 0.104 µM for the observations. Compared to the Control optimisation (Fig. 2A), in the Oyster optimisation the amplitude of the daily variations was low (Fig. 3A), and over the entire period the concentration ranged from a minimum of 0.07 µM to a maximum of 0.17 µM.

Similarly, the PO_4^{3-} concentration (Fig. 3B) of the Oyster optimisation was more similar to that of the observations than was the concentration in the Oyster initial simulation. This similarity was particularly pronounced for the second half of the experimental period, when the concentration varied between 0.02 and 0.29 µM. The daily variations occurring until Day 3 were greater compared with those on the following days.

The SiO_4^{2-} concentration (Fig. 3C) in the optimised simulation was more similar to that of the observations than the concentration in the initial simulation. The trend was also better than that in the initial simulation. The SiO_4^{2-} concentration decreased until Day 3 and remained almost constant thereafter, with a slight increase to 6.77 µM at the end of the experiment relative to the concentration of 6.35 µM observed in the mesocosms.

With the addition of oysters, the NH_4^+ concentration (Fig. 7A) exhibited an ever-increasing trend in the Oyster optimisation, varying from 1.20 µM in the Oyster initial simulation to 2.73 µM in the optimised simulation on Day 2. At the end, the simulated NH_4^+ concentration was 10.91 µM.

The optimised simulated DOC concentration (Fig. 3D) showed a slight decrease and then increased more than that in the Oyster initial simulation to be more similar to that observed in the mesocosms. However, the simulated concentrations were much lower than the observed concentrations. The average DOC concentration over the entire period

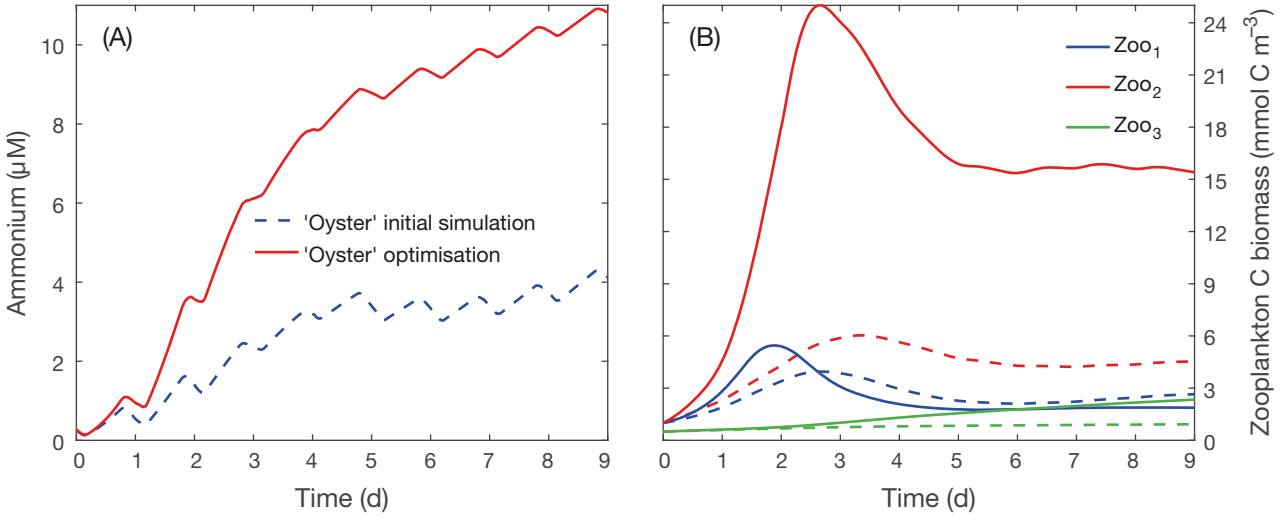

Fig. 7. Comparison between the Oyster initial simulation and Oyster optimisation for concentrations of (A) ammonium and (B) zooplankton C biomass. The 3 compartments of zooplankton are represented: Zoo_1 (mostly bacterivorous flagellates and small ciliates), Zoo_2 (mainly ciliates and large flagellates), and Zoo_3 (metazooplankton dominated by copepods)

was 214.07 µM for the optimised simulation and 261.73 µM for the observations.

From Day 0 to Day 2, the chl *a* concentration (Fig. 3E) for the Oyster optimisation exhibited the same increase observed in the mesocosms, with an amplitude of daily variations of 1.2 mg m^{-3}. It decreased sharply on Day 3 and periodically fluctuated thereafter. The maximum value in the optimised simulation, reached on Day 1, was 3.88 mg m^{-3}. Between Days 5 and 9, the average concentration was 0.98 mg m^{-3}, compared to 0.20 mg m^{-3} for the observations.

The bacterial C biomass concentration (Fig. 3F) in the optimised simulation was more similar to that for the observations than that in the initial simulation. It increased from Day 0 until the end of Day 1, where it reached a maximum of 21.87 mmol C m^{-3}. Then, a quick decrease was simulated until Day 3. However, for the Oyster optimisation, the simulated bacterial C biomass concentration remained lower than the observed concentration from Day 4 until the end of the experiment.

Concerning the zooplankton C biomass concentration (Fig. 7B), after Day 3, Zoo_2 largely dominated the zooplankton community. Its concentration reached a maximum of 25.00 mmol C m^{-3} on Day 3. The concentration in the optimised simulation followed a similar scheme as that in the Control simulation without oysters, with succession of domination by the different zooplankton classes. However, the spikes appeared earlier in the simulation. The Zoo_3 C biomass concentration was increased by the optimisation process. At the end of the experimental period, the C biomass concentrations of Zoo_1, Zoo_2, and Zoo_3 were 1.88, 15.41, and 2.34 mmol C m^{-3}, respectively.

Fig. 8 shows the temporal evolution of oyster C biomass ([Oyster]C) during the 10 d of the experiment, revealing a regular increase from the beginning until the end of the experiment of 9.2–16.5 mmol C m^{-3}. The only information that we had at the beginning of the experiment was the introduction of 10 oysters into each mesocosm. This initial condition was highly speculative, and this led to careful consideration of the optimised value obtained for the filtration rate

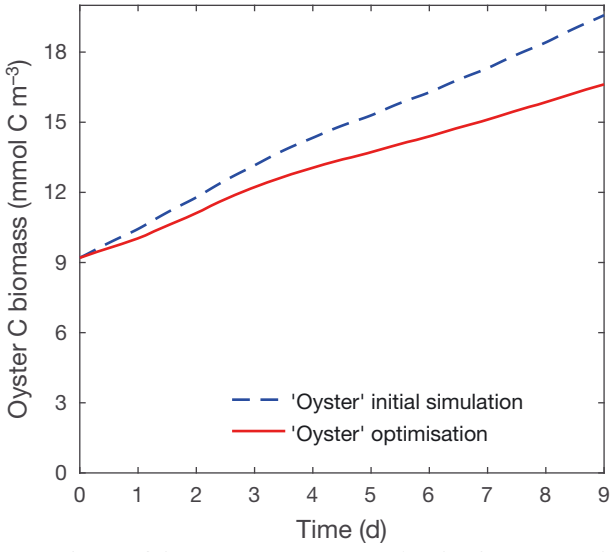

Fig. 8. Oyster C biomass concentration for the Oyster initial simulation and Oyster optimisation

parameter after optimisation. The adjustment of this initial condition for oyster C biomass should result in an adjustment of oyster parameters.

3.2.2. Analysis of adjusted parameters

The optimisation procedure led to the calibration of the 180 parameters, including the new parameters for oysters, as detailed in Table 2. Table 4 shows that the key parameters changed during the optimisation according to their resolution. The new Oyster parameters did not have the highest resolution values (see Table 2). However, as expected, $filt_0$, $effO_{Phy3}$, and $bd_{\%}$ changed very slightly during the process.

Two of these key parameters concerned bacterial processes (Table 4). The maximum uptake rate for bacteria greatly increased, from 1.97–2.87 × 10^{-5} s^{-1}, contributing to the increase in bacterial C biomass concentration (Fig. 3F). Furthermore, DOM transformation into inorganic nutrients greatly increased. The bacterial P:C ratio also changed during the optimisation process, affecting the consumption of PO_4^{3-} by bacteria.

Six key parameters concerned the processes of the phytoplankton community (Table 4). The modification of 2 of them during optimisation affected the growth of the phytoplankton community. First, the maximal internal chl:N ratio for Phy increased, which resulted in a faster increase in the chl *a* concentration for the Oyster optimisation than for the Oyster initial simulation. In contrast, the increase in the half-saturation constant for NO_3^- uptake from 2.24–4.66 µM tended to decrease the growth of the phytoplankton community at a constant NO_3^- concentration (Fig. 3A). These 2 changes had opposite effects, but the results showed higher growth for Phy (Fig. 3E). This discrepancy could be related to the fact that the maximal internal chl:N ratio had a higher resolution value (0.84 vs. 0.38), i.e. higher importance in the optimisation procedure. The maximal Si:C ratio also decreased, from 0.38–0.28 mol Si (mol C)$^{-1}$. This modification caused the diminution of the SiO_4^{2-} concentration after Day 3 (Fig. 3C) for the optimised simulation compared to the Oyster initial simulation, even if the chl *a* concentration remained low (Fig. 3E).

In the same manner as in the Control optimisation, 7 parameters linked with zooplankton processes are shown in Table 4. The parameters presented both a high resolution and a significant change during the optimisation procedure and concerned different processes. For example, the maximal grazing rate of Zoo_2 and the preference factor of Zoo_2 for bacteria concerned predation by zooplankton and thus their prey, whereas the fraction of messy feeding for zooplankton concerned their messy feeding and thus light and heavy non-living POM concentrations.

3.2.3. Analysis of data resolution

In the Oyster optimisation, the data resolution results were very different from those in the Control optimisation. According to Fig. 6B, on average the PO_4^{3-}, and SiO_4^{2-} data resolutions were the highest, while the resolutions of the NO_3^-, chl *a*, and bacteria data were almost equal. During the experimental period, the resolution for each observation showed great variation.

Table 4. Key parameters changed during the Oyster optimisation process assimilating Oyster mesocosm observations. DOC: dissolved organic carbon; Phy: phytoplankton; Zoo: zooplankton

Name	Initial value	Final value	Units	Resolution
Maximum uptake rate of bacteria for DOC	1.97 × 10^{-5}	2.87 × 10^{-5}	s^{-1}	0.84
Maximal internal Si:C ratio of Phy	0.38	0.28	mol Si (mol C)$^{-1}$	0.63
Maximal internal chl:N ratio of Phy	2.03	2.24	mg chl (mmol N)$^{-1}$	0.51
Reference temperature for zooplankton processes	12.50	11.52	°C	0.49
Ratio of small/large organic matter in dead zooplankton	0.99	1.09	–	0.48
Fraction of messy feeding for zooplankton	0.31	0.27	–	0.42
Maximal internal N:C ratio of Phy	0.19	0.13	mol N (mol C)$^{-1}$	0.40
P:C ratio of bacteria	0.94 × 10^{-2}	1.32 × 10^{-2}	mol P (mol C)$^{-1}$	0.38
Ratio of small/large particulate organic matter in dead Phy	0.82	0.87	–	0.36
Maximal grazing rate of Zoo_2	5.60 × 10^{-5}	5.49 × 10^{-5}	s^{-1}	0.32
Preference factor of Zoo_2 for bacteria	6.98 × 10^{-2}	6.18 × 10^{-2}	–	0.31
Half-saturation constant for nitrate uptake for Phy	2.24	4.66	mmol N m^{-3}	0.30
Fixed P:C ratio of Zoo_2	1.44 × 10^{-2}	1.51 × 10^{-2}	mol P (mol C)$^{-1}$	0.30
Maximal internal P:C ratio of Phy	2.85 × 10^{-2}	3.55 × 10^{-2}	mol P (mol C)$^{-1}$	0.27
Fixed N:C ratio of Zoo_2	0.19	0.14	mol N (mol C)$^{-1}$	0.24

The chl *a* data resolution was high on Days 1 and 3, at 0.53 and 0.84, respectively, but remained low thereafter. The chl *a* data resolution was the highest on Day 4. The NO_3^- data resolution was high on Days 1, 3, and 7. It reached a maximum on Day 7, at 0.99. The PO_4^{3-} data resolution was very high on Days 2 and 3, reaching 0.98 on Day 3. It was almost constant at approximately 0.25 during the last few days of the experiment. The SiO_4^{2-} data resolution was also high on Days 1, 7, and 9, when it reached a very high value of approximately 0.93. The DOC data resolution remained very low during the experimental period, except on Day 9, when it was 0.79. The DOC data made the smallest contribution to the optimisation process. The bacterial data resolution was higher on Day 2, at 0.69, than on the other days of the experiment but made a good contribution to the optimisation during the entire period of the experiment.

4. DISCUSSION

To assess the impact of oysters as top predators in MFW dynamics, a modelling approach with parameter optimisation was applied. The Eco3m-S biogeochemical model, coupled with the optimisation method presented in Section 2.3, efficiently reproduced observations made during a mesocosm experiment. The optimisation method estimated a linear combination of parameters giving the best compatibility with the 6 different observations (NO_3^-, PO_4^{3-}, SiO_4^{2-}, DOC, chl *a*, and bacterial C biomass). Finding a solution for the assimilation process is not a simple curve-fitting procedure because of the complexity and non-linearity of the interactions among the compartments of the model. Once the new biogeochemical model including oysters was validated, the impact of oysters on the MFW was investigated by studying the structural changes in the MFW and the interactions within the MFW.

4.1. The potential of parameter optimisation

The parameter resolution resulting from the optimisation method reflected the importance of each biogeochemical process in the model. Using this new benefit, the biogeochemical processes could be sorted by importance. For example, in our modelling experiment, bacterial processes played a very important role in MFW dynamics. Indeed, in both the Control and Oyster optimisations, the maximum uptake rate for bacteria exhibited the highest resolution of the entire set of control parameters (see Tables 3 & 4), in line with the major role played by bacteria in the marine C cycle (e.g. Cho & Azam 1988, Azam et al. 1994).

In contrast, the low resolution of the control parameters of the new oyster compartment, with a maximum of 0.08 (Table 2), showed that changing associated processes was not beneficial for the optimisation process. However, the fact that parameter values did not change during optimisation might indicate that the choice of initial values was robust and that these values could thus be used for further studies.

To meet the mathematical requirements of the optimisation method, some of the most influential parameters, i.e. those with the highest resolutions, were modified by optimisation and reached unrealistic values. These unrealistic values allowed the simulated results to be more similar to the experimental observations by minimising the cost function more efficiently. This was the case for the net growth efficiency for bacteria and 3 other parameters controlling temperature functions: the reference temperature for zooplankton, the reference temperature for decomposition, and the temperature coefficient for decomposition. The optimisation method preferred changing one parameter controlling the temperature functions, affecting several temperature-dependent processes at the same time, over changing multiple parameters controlling only one process each. Note that the parameters controlling temperature functions generally had a high resolution value. Furthermore, unrealistic values could be explained with a deeper analysis of other parameter values. According to the scientific literature, the net growth efficiency for bacteria should be between 0.05 and 0.7 (Del Giorgio & Cole 1998). However, considering that bacterial growth depends on the product of this parameter value with the value of the maximal uptake rate of bacteria, the decrease in the maximal uptake rate of bacteria during the optimisation process partially balanced the increase in the net growth efficiency for bacteria. For example, for the Control optimisation, the product varied from $1.28–1.95 \times 10^{-5}$ s^{-1}. Indeed, the optimisation process modified a linear combination of parameters and not individual parameters.

Data resolution, also resulting from optimisation, can be of interest for managing experimental efforts in order to build more realistic modelling studies. They reflect the contribution of each assimilated data point as useful information for the optimisation method. For instance, chl *a* and bacterial C biomass were very important to render the biogeochemical model closer to observations, in the case where the

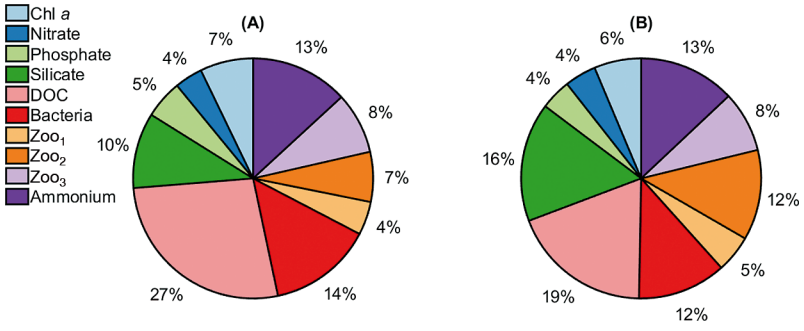

Fig. 9. Data resolution calculated for each type of observation, averaged over the experimental period, for the (A) Control and (B) Oyster optimisations, in the case where the 10 indicated observations were available. DOC: dissolved organic carbon; Zoo_1: bacterivorous flagellates and small ciliates; Zoo_2: ciliates and large flagellates; Zoo_3: metazooplankton dominated by copepods

method assimilated only 6 variables (Fig. 6). Following these results, a new modelling experiment was performed, assuming the method of assimilating zooplankton biomass and NH_4^+ in addition to the previous 6 variables. The calculation of data resolution for these new observable outputs was then made (Fig. 9). The results highlight the fact that, in the case where those 10 variables would be assimilated, NH_4^+ and zooplankton biomass are key variables for improving the ecological model, as well as DOC concentration. Therefore, the management of observational efforts for realistic modelling not only depends on the study area and biogeochemical model, but also on the assimilated variables.

4.2. Oysters induced structural changes in the MFW

The introduction of oysters as top predators of the MFW led to a more heterotrophic ecosystem. The structural A:H C biomass ratio index (Fig. 10) was calculated and compared to results from Mostajir et al. (2015). This calculation was simple with the model, which estimated the C biomass of each biological component of the model compared to experimental calculations, which were associated with strong uncertainties because of the C biomass calculation method. The gap between the 2 simulations was less important than the gaps associated with the experimental study, but the results were in the same direction. Overall, the experimental MFW was well represented by the model, at least structurally, with only 6 types of experimental observations assimilated. Therefore, the model corroborated the tendency for a transition to a more heterotrophic MFW with the addition of oysters as top predators, which could be useful for testing scenarios with the model. For example, the model could be used to simulate a scenario with a higher quantity of oysters to assess the structural impact of more intensive exploitation.

The main function of oysters in our model was filtering all mesocosm water containing living and non-living organisms. Fig. 11 shows the filtration of each MFW component, resulting from Eq. (10). According to the parameters used to define the filtration rate, the most filtered compartment corresponded to the phytoplankton community. Zooplankton was the second most filtrated, and light non-living POM and bacteria were the third most filtrated. Our model included the direct reduction of phytoplankton biomass by oysters by adding a new filtration term, $filt_{Phy}$. This result was in line with those of Cugier et al. (2010) and Mostajir et al. (2015). Nevertheless, this process also indirectly impacted other components of the MFW, such as zooplankton, which may find fewer prey in the phytoplankton community.

The simulated phytoplankton biomass was approximately 30% lower than the phytoplankton biomass in the Control optimisation (Fig. 2E vs. Fig. 3E).

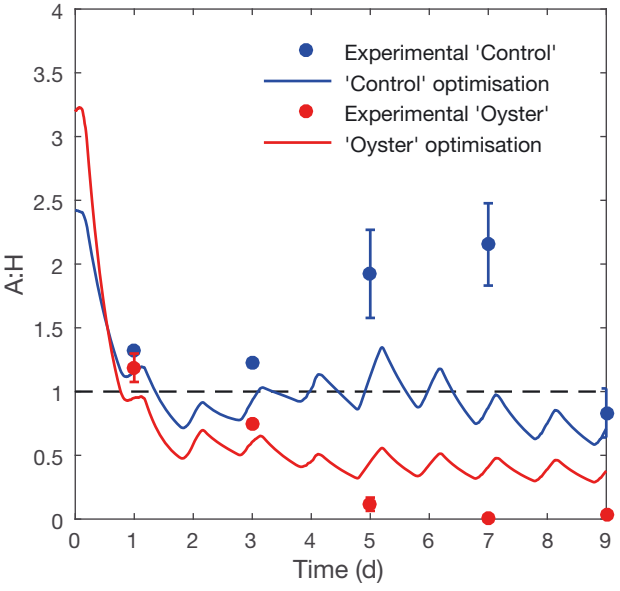

Fig. 10. Autotroph:heterotroph (A:H) structural index comparison between the mesocosm experimental study (points are means with whiskers showing range, n = 2) and biogeochemical modelling (solid lines) for the Control and Oyster optimisations

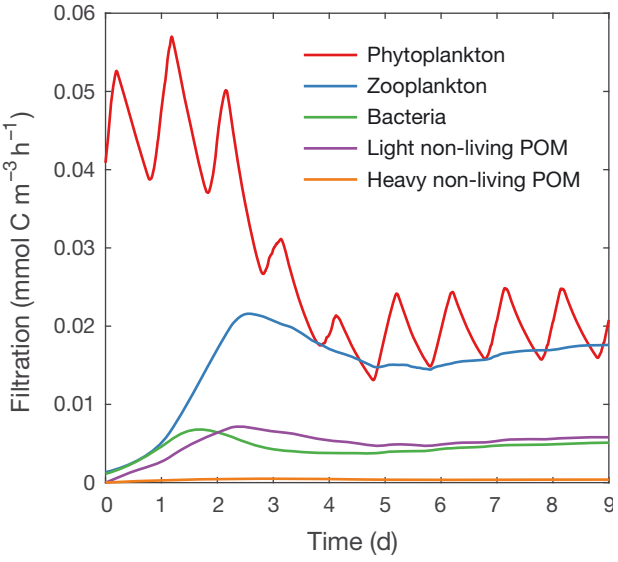

Fig. 11. Filtration by oysters of other components of the microbial food web: phytoplankton, zooplankton, bacteria, light non-living particulate organic matter (POM), and heavy non-living POM

The bacterial biomass was also affected, being 50% greater than that in the Control optimisation (Fig. 2F vs. 3F). Oysters strongly increased zooplankton biomass by approximately 110% (Fig. 5B vs. 7B). Therefore, the increase in the biomass of zooplankton and reduction in the biomass of phytoplankton, which are prey of zooplankton, could be in line with top-down control. The simulated predation of phytoplankton by zooplankton was slightly higher in the Oyster optimisation than in the Control optimisation (data not shown), but this result does not fully explain the large increase in zooplankton biomass. However, the reduction in phytoplankton biomass is explained by the top-down control of oysters but also by the increased predation of zooplankton. Losey & Denno (1998) showed that the combined influence of 2 predators could be greater than the sum of their individual impacts. Here, the combined influence of oyster and zooplankton biomasses on phytoplankton biomass was greater than the sum of the individual impacts.

The introduction of a top predator to an ecosystem could lead to unexpected results; in particular, the introduction of an alien top predator could have a devastating impact on native species (e.g. Bytheway et al. 2016). In our case, we cannot exclude this possibility for the Thau lagoon ecosystem, where non-native oysters (*Crassostrea gigas*, a Japanese oyster) have been cultivated since 1972 (Hamon et al. 2003), because oysters exert strong structural control of the natural lagoon MFW community.

4.3. Indirect impact of oysters on bacterial biomass

Simulated bacterial biomass strongly increased in the presence of oysters as top predators of the MFW, in accordance with the study of Mostajir et al. (2015). Those authors proposed different hypotheses to explain the increase in bacteria, and some of the hypotheses can be discussed based on the new modelling results acquired here. First, bacteria might benefit from oyster excreta (Mazouni et al. 1998), but since the excreta of oysters was not modelled in this study and simulated bacterial biomass was similar to that in the experimental observations, this benefit might not explain the increase. Second, Mostajir et al. (2015) highlighted the assumption that the reduction in virus-like particles due to oyster filtration could favour an increase in bacterial biomass. However, viruses were not modelled, particularly due to the complexity of their interactions with other components of the MFW, and this assumption was not investigated.

Our results support the third hypothesis posed by Mostajir et al. (2015), concerning the reduction in competition between bacteria and phytoplankton for the uptake of nutrients. To quantify competition between bacteria and phytoplankton, nutrient uptake fluxes were analysed. Fig. 12 shows the comparison between Control and Oyster optimisations for NH_4^+ (Fig. 12A) and PO_4^{3-} uptake (Fig. 12B) by phytoplankton. For bacteria, the same comparison is shown for NH_4^+ uptake (Fig. 12C) and PO_4^{3-} excretion (Fig. 12D). The model version of Auger et al. (2011) includes potential control of bacterial growth by P availability, in addition to limitation by C and N availability. This model formulation is derived from Thingstad et al. (1998). Bacteria first absorb DOM, but they can also assimilate NH_4^+ and/or PO_4^{3-} if dissolved organic nitrogen and/or phosphorus (DON and DOP) are lacking. Bacteria can also act as decomposers and excrete nutrients, depending on the comparison of DOC:DON and/or DOC:DOP with their internal ratios (Kirchman et al. 2000). All the processes (nutrient uptake, excretion, and respiration) make the control of their stoichiometry possible. Our results showed that, except for PO_4^{3-} uptake, phytoplankton nutrient uptake was lower with the addition of oysters (Fig. 12A,B). Furthermore, in contrast to the pattern observed in the Control optimisation, where no NH_4^+ bacterial uptake was observed (Fig. 12C), bacterial NH_4^+ uptake increased in the Oyster optimisation after Day 7. It can be concluded that competition

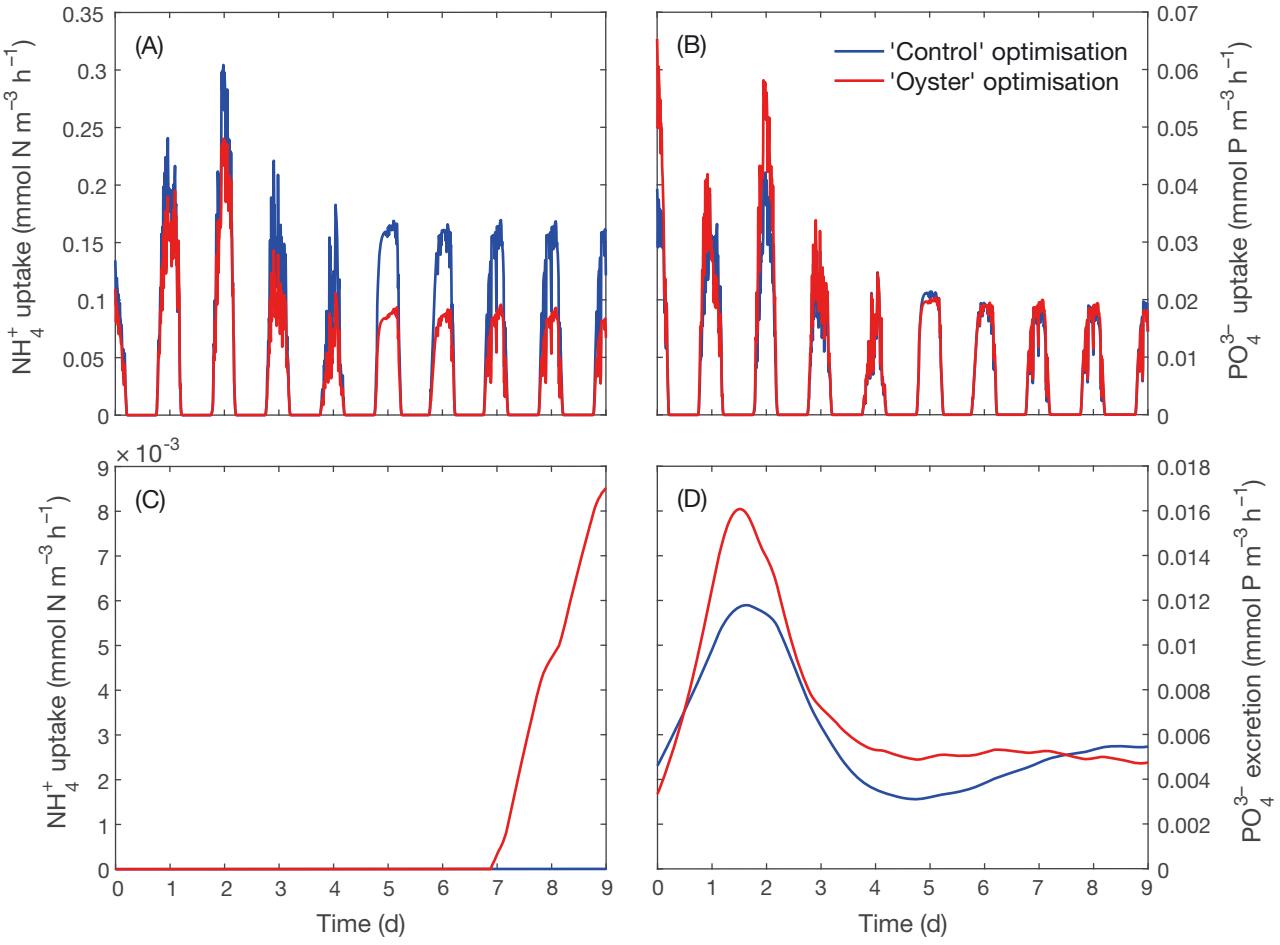

Fig. 12. Comparison between the Control and Oyster optimisations for the (A) uptake of ammonium by phytoplankton, (B) uptake of phosphate by phytoplankton, (C) uptake of ammonium by bacteria, and (D) excretion of phosphate by bacteria

between bacteria and phytoplankton was reduced in our model, especially for NH_4^+. In addition, the excretion of PO_4^{3-} by bacteria was higher with oysters and conveniently balanced the higher PO_4^{3-} needs of the phytoplankton community. Thingstad et al. (2007) showed that the dynamics of a water column receiving NO_3^-, PO_4^{3-}, and DOC continuously shift to lower nutrient competition and higher nutrient regeneration. The introduction of oysters slightly increased the DOC, NO_3^-, and PO_4^{3-} concentrations in the water column, which could correspond to the case studied by Thingstad et al. (2007).

Our results showed that the reduction in this competition benefited both bacterial and phytoplankton growth. However, the phytoplankton community was subject to other strong constraints, such as filtration by oysters, as explained above. Thus, the larger quantity of nutrients available for bacteria actually resulted in more bacterial biomass in the Oyster simulation.

4.4. Impact of oysters on the zooplankton community

The increase in bacterial biomass in the Oyster simulation favoured an increase in bacterivorous zooplankton biomass (mainly Zoo_1 but also Zoo_2 in a smaller proportion). However, the Zoo_1 C biomass slightly decreased with the addition of oysters (Fig. 5B vs. Fig. 7B). The maximum Zoo_1 C biomass of the Oyster optimisation was 5.46 mmol C m^{-3} and was reached at the beginning of Day 2. On the same date in the Control simulation, the Zoo_1 C biomass was 4.41 mmol C m^{-3}. This result supports the idea that the increase in bacterial biomass favoured bacterivorous zooplankton because the growth of Zoo_1 was higher in the presence of oysters.

The high Zoo_1 C biomass obtained in the presence of oysters led to a direct increase in the C biomass of Zoo_2. Thus, Zoo_1 served as a link between bacteria and Zoo_2. Moreover, our results showed an increase

in Zoo_2 in the Oyster simulation that was faster than the increase in Zoo_1 (Fig. 7B). Indeed, the predation pressure of Zoo_2 on Zoo_1 was higher than the predation pressure of Zoo_1 on bacteria (data not shown).

Therefore, in the presence of oysters, the phytoplankton community (the main source of food for oysters) was greatly impacted by direct oyster filtration. Bacteria benefited from the reduction of phytoplankton community biomass through the reduction in competition between bacteria and phytoplankton for nutrient uptake. This increase in bacterial biomass favoured bacterivorous zooplankton (Zoo_1), which were preyed upon by Zoo_2. Finally, this phenomenon resulted in a higher Zoo_2 biomass in the Oyster simulation than in the Control simulation. This result could be compared to the 'minimum model' of Thingstad et al. (2007), where ciliates (Zoo_2) and bacterial abundances were positively correlated through the heterotrophic flagellates (Zoo_1) link. However, in the 'minimum model' the top-down control from copepods (Zoo_3) tended to stimulate diatoms, whereas in our model the insertion of oysters resulted in a reduction of the phytoplankton community.

The modelling approach provided a real advantage in investigating the interactions between different components of the MFW. The use of a mechanistic formulation of biogeochemical processes (see Section 2.2) renders the extraction of stocks and fluxes simple. This discussion focused on filtration by oysters (Fig. 11), predation by zooplankton, and competition between phytoplankton and bacteria for nutrients (Fig. 12). These biogeochemical fluxes, easily extracted from the simulation results, provide a great deal of new information for our understanding of the impact of oysters as top predators of the MFW.

5. CONCLUSIONS

In this study, numerical ecosystem simulations with the Eco3m-S model were performed to provide deeper insight into the interactions and fluxes within the MFW. A parameter optimisation method assimilating mesocosm experimental observations described in Mostajir et al. (2015) was used, and the model efficiently reproduced observations with and without oysters. The model provided high-frequency results over the period of the experiment, and fluxes within the MFW were extracted and analysed. For example, the comparison of nutrient uptake by bacteria and the phytoplankton community brought to light a decrease in competition for nutrients between these 2 components of the MFW in the presence of oysters. Due to the filtration of all mesocosm water including organisms and non-living particles, the direct and immediate impact of oysters was mainly a reduction in phytoplankton C biomass. In addition, our results showed an increase in zooplankton and bacterial biomasses. The mesocosms thus became more heterotrophic with oysters. The reduction in competition for nutrients between bacteria and phytoplankton, as mentioned above, resulted in higher bacterial biomass in the Oyster simulation. The increase in zooplankton biomass was explained by a strong increase in simulated Zoo_2 biomass (50–200 µm; mainly ciliates and large flagellates) due to the grazing of Zoo_1 bacterivorous zooplankton (5–50 µm; mostly bacterivorous flagellates and small ciliates), which appeared as an intermediary trophic link. In our study, oysters pushed the system to a more heterotrophic state with higher micro-zooplankton and bacterial C biomasses and lower phytoplankton C biomass.

Modelling, observation, and experimentation are complementary for obtaining a good understanding of ecological processes. Observation and experimentation provide a real but partial view of the processes involved, and the ideal scenario in which everything could be observed or monitored persists. Modelling approaches provide estimates more or less close to reality, depending on the quality of known assumptions. However, such approaches often yield information that is more complete and has a greater temporal resolution. Models are fed with theories and observations. The modelling approach introduces a new point of view, which is useful for understanding biogeochemical mechanisms, paying attention to assumptions made beforehand. In our case, we succeeded in reproducing not only the steady state of the observed mesocosm experiment but also the dynamics of the ecosystem over the 10 d experimental period. Additional information was provided by the model, such as biogeochemical fluxes within the MFW. This idea should encourage the scientific community to pursue more interactions between modelling, observations, and experimental communities.

Analysing data assimilated during the optimisation process could also be a simple way to define the most interesting data required for the modelling approach. It could help manage experimental efforts in order to conduct a more realistic modelling study. For example, in our study, data available for chl *a* or bacteria were very important for the Control optimisation. Furthermore, our results were very similar to mesocosm observations and suggest that NH_4^+ observations, which were not available, were not essential in this specific case. Data resolutions also contain tem-

poral information that reveals, for example, if it is better to measure each variable once a day or measure one variable at a high frequency and others at a low frequency. The answer strongly depends on the system's dynamics and the complexity of the processes involved. Regarding our results, a good effort to obtain numerous chl *a* observations was needed compared to DOC observations, which, for example, could be measured only once a week.

Acknowledgements. This work was supported by the CNRS-INSU project 'CHIFRE' and a PhD grant from the Montpellier University. We also thank the American Journal Expert company for reviewing the English.

LITERATURE CITED

Auger PA, Diaz F, Ulses C, Estournel C and others (2011) Functioning of the planktonic ecosystem on the Gulf of Lions shelf (NW Mediterranean) during spring and its impact on the carbon deposition: a field data and 3-D modelling combined approach. Biogeosciences 8: 3231–3261

Auger PA, Ulses C, Estournel C, Stemmann L, Somot S, Diaz F (2014) Interannual control of plankton communities by deep winter mixing and prey/predator interactions in the NW Mediterranean: results from a 30-year 3D modeling study. Prog Oceanogr 124:12–27

Azam F, Smith DC, Steward GF, Hagström Å (1994) Bacteria-organic matter coupling and its significance for oceanic carbon cycling. Microb Ecol 28:167–179

Barillé L, Prou J, Héral M, Bourgrier S (1993) No influence of food quality, but ration-dependent retention efficiencies in the Japanese oyster *Crassostrea gigas*. J Exp Mar Biol Ecol 171:91–106

Bayne BL (2017) Feeding. In: Osborn P (ed) Biology of oysters. Developments in aquaculture and fisheries science, Vol 41. Academic Press, London, p 209–330

Bytheway JP, Price CJ, Banks PB (2016) Deadly intentions: naïve introduced foxes show rapid attraction to odour cues of an unfamiliar native prey. Sci Rep 6:30078

Callier MD, Weise AM, McKindsey CW, Desrosiers G (2006) Sedimentation rates in a suspended mussel farm (Great-Entry Lagoon, Canada): biodeposit production and dispersion. Mar Ecol Prog Ser 322:129–141

Callier MD, Richard M, McKindsey CW, Archambault P, Desrosiers G (2009) Responses of benthic macrofauna and biogeochemical fluxes to various levels of mussel biodeposition: An *in situ* 'benthocosm' experiment. Mar Pollut Bull 58:1544–1553

Chapelle A, Ménesguen A, Deslous-Paoli JM, Souchu P, Mazouni N, Vaquer A, Millet B (2000) Modelling nitrogen, primary production and oxygen in a Mediterranean lagoon. Impact of oysters farming and inputs from the watershed. Ecol Model 127:161–181

Cho BC, Azam F (1988) Major role of bacteria in biogeochemical fluxes in the ocean's interior. Nature 332: 441–443

Cugier P, Struski C, Blanchard M, Mazurié J and others (2010) Assessing the role of benthic filter feeders on phytoplankton production in a shellfish farming site: Mont Saint Michel Bay, France. J Mar Syst 82:21–34

De Crignis M (2007) Sources de nourriture et bio-énergétique de l'huître creuse *Crassostrea gigas*: les nanoflagellés et les ciliés jouent-ils un rôle dans le budget d'énergie dynamique d'huîtres. MSc dissertation, Université de La Rochelle

Defossez JM, Hawkins AJS (1997) Selective feeding in shellfish: size-dependent rejection of large particles within pseudofaeces from *Mytilus edulis*, *Ruditapes philippinarum* and *Tapes decussatus*. Mar Biol 129:139–147

Del Giorgio PA, Cole JJ (1998) Bacterial growth efficiency in natural aquatic systems. Annu Rev Ecol Syst 29:503–541

Duarte P, Meneses R, Hawkins AJS, Zhu M, Fang J, Grant J (2003) Mathematical modelling to assess the carrying capacity for multi-species culture within coastal waters. Ecol Model 168:109–143

Dupuy C, Le Gall S, Hartmann HJ, Bréret M (1999) Retention of ciliates and flagellates by the oyster *Crassostrea gigas* in French Atlantic coastal ponds: protists as a trophic link between bacterioplankton and benthic suspension-feeders. Mar Ecol Prog Ser 177:165–175

Dupuy C, Vaquer A, Lam-Höai T, Rougier C and others (2000) Feeding rate of the oyster *Crassostrea gigas* in a natural planktonic community of the Mediterranean Thau Lagoon. Mar Ecol Prog Ser 205:171–184

Frikha MG, Linley EAS, Delmas D (1987) Evolution annuelle et saisonnière de la microbiomasse d'une claire à huîtres: importance des populations bactérioplanctoniques. Oceanis 13:433–447

Froján M, Arbones B, Zúñiga D, Castro CG, Figueiras FG (2014) Microbial plankton community in the Ría de Vigo (NW Iberian upwelling system): impact of the culture of *Mytilus galloprovincialis*. Mar Ecol Prog Ser 498:43–54

Gangnery A, Bacher C, Buestel D (2001) Assessing the production and the impact of cultivated oysters in the Thau lagoon (Mediterranee, France) with a population dynamics model. Can J Fish Aquat Sci 58:1012–1020

Gangnery A, Chabirand JM, Lagarde F, Le Gall P, Oheix J, Bacher C, Buestel D (2003) Growth model of the Pacific oyster, *Crassostrea gigas*, cultured in Thau Lagoon (Méditerranée, France). Aquaculture 215:267–290

Gangnery A, Bacher C, Buestel D (2004) Modelling oyster population dynamics in a Mediterranean coastal lagoon (Thau, France): sensitivity of marketable production to environmental conditions. Aquaculture 230:323–347

Gonzalez Vicente P (1986) Recherche de la dimension de l'espace latent en ACP. Stat Anal Données 11:19–29

Gosling E (2015) How bivalves feed. In: Marine bivalve molluscs. John Wiley & Sons, Chichester, p 99–156

Grant J, Bacher C, Cranford PJ, Guyondet T, Carreau M (2008) A spatially explicit ecosystem model of seston depletion in dense mussel culture. J Mar Syst 73:155–168

Hamon PY, Vercelli C, Pichot Y, Lagarde F, Le Gall P, Oheix J (2003) Les malaïgues de l'étang de Thau. Tome 1. Description des malaïgues. Moyens de lutte, Recommandations. Archive Ifremer, Sete Cedex

Haven DS, Morales-Alamo R (1966) Aspects of biodeposition by oysters and other invertebrate filter feeders. Limnol Oceanogr 11:487–498

Ibarra DA, Fennel K, Cullen JJ (2014) Coupling 3-D Eulerian bio-physics (ROMS) with individual-based shellfish ecophysiology (SHELL-E): a hybrid model for carrying capacity and environmental impacts of bivalve aquaculture. Ecol Model 273:63–78

Jansen HM, Strand Ø, Strohmeier T, Krogness C, Verdegem M, Smaal A (2011) Seasonal variability in nutrient regen-

eration by mussel *Mytilus edulis* rope culture in oligotrophic systems. Mar Ecol Prog Ser 431:137–149

Kirchman DL, Meon B, Cottrell MT, Hutchins DA, Weeks D, Bruland KW (2000) Carbon versus iron limitation of bacterial growth in the California upwelling regime. Limnol Oceanogr 45:1681–1688

Kooijman SALM (1986) Energy budgets can explain body size relations. J Theor Biol 121:269–282

Kooijman SALM (2000) Dynamic energy and mass budgets in biological systems, 2nd edn. Cambridge University Press, Cambridge

Kooijman B (2009) Dynamic energy budget theory for metabolic organisation, 3rd edn. Cambridge University Press, Cambridge

Le Gall JL, Raillard O (1988) Influence de la température sur la physiologie de l'huître *Crassostrea gigas*. Oceanis 14: 603–608

Le Gall S, Hassen MB, Le Gall P (1997) Ingestion of a bacterivorous ciliate by the oyster *Crassostrea gigas*: protozoa as a trophic link between picoplankton and benthic suspension-feeders. Mar Ecol Prog Ser 152:301–306

Losey JE, Denno RF (1998) Positive predator–predator interactions: enhanced predation rates and synergistic suppression of aphid populations. Ecology 79:2143–2152

Marinov D, Galbiati L, Giordani G, Viaroli P, Norro A, Bencivelli S, Zaldívar JM (2007) An integrated modelling approach for the management of clam farming in coastal lagoons. Aquaculture 269:306–320

Mazouni N (1995) Influence des élevages ostréicoles sur le fonctionnement d'un écosystème lagunaire méditerranéen. Etude in situ de l'influence des filtreurs (coquillages et épibiontes) sur les flux de matières particulaire et dissoute. PhD dissertation, Université Aix-Marseille II, Marseille

Mazouni N (2004) Influence of suspended oyster cultures on nitrogen regeneration in a coastal lagoon (Thau, France). Mar Ecol Prog Ser 276:103–113

Mazouni N, Gaertner JC, Deslous-Paoli JM, Landrein S, Geringer d'Oedenberg M (1996) Nutrient and oxygen exchanges at the water–sediment interface in a shellfish farming lagoon (Thau, France). J Exp Mar Biol Ecol 205: 91–113

Mazouni N, Gaertner JC, Deslous-Paoli JM (1998) Influence of oyster culture on water column characteristics in a coastal lagoon (Thau, France). In: Amiard JC, Le Rouzic B, Berthet B, Bertru G (eds) Oceans, rivers and lakes: energy and substance transfers at interfaces. Springer, Dordrecht, p 149–156

Mostajir B, Roques C, Bouvier C, Bouvier T and others (2015) Microbial food web structural and functional responses to oyster and fish as top predators. Mar Ecol Prog Ser 535:11–27

Plus M, Auby I, Maurer D, Trut G, Del Amo Y, Dumas F, Thouvenin B (2015) Phytoplankton versus macrophyte contribution to primary production and biogeochemical cycles of a coastal mesotidal system. A modelling approach. Estuar Coast Shelf Sci 165:52–60

Prunet P, Minster JF, Ruiz-Pino D, Dadou I (1996) Assimilation of surface data in a one-dimensional physical-biogeochemical model of the surface ocean. 1. Method and preliminary results. Global Biogeochem Cycles 10:111–138

Richard M, Archambault P, Thouzeau G, McKindsey CW, Desrosiers G (2007) Influence of suspended scallop cages and mussel lines on pelagic and benthic biogeochemical fluxes in Havre-aux-Maisons Lagoon, Îles-de-la-Madeleine (Quebec, Canada). Can J Fish Aquat Sci 64: 1491–1505

Richard M, Bec B, Vanhuysse C, Mas S and others (2019) Changes in planktonic microbial components in interaction with juvenile oysters during a mortality episode in the Thau lagoon (France). Aquaculture 503:231–241

Robert P, Mckindsey CW, Chaillou G, Archambault P (2013) Dose-dependent response of a benthic system to biodeposition from suspended blue mussel (*Mytilus edulis*) culture. Mar Pollut Bull 66:92–104

Sherman E, Moore JK, Primeau F, Tanouye D (2016) Temperature influence on phytoplankton community growth rates. Global Biogeochem Cycles 30:550–559

Sime-Ngando T, Gosselin M, Roy S, Chanut JP (1995) Significance of planktonic ciliated protozoa in the Lower St. Lawrence Estuary: comparison with bacterial, phytoplankton, and particulate organic carbon. Aquat Microb Ecol 9:243–258

Souchu P, Vaquer A, Collos Y, Landrein S, Deslous-Paoli JM, Bibent B (2001) Influence of shellfish farming activities on the biogeochemical composition of the water column in Thau lagoon. Mar Ecol Prog Ser 218:141–152

Spillman CM, Hamilton DP, Hipsey MR, Imberger J (2008) A spatially resolved model of seasonal variations in phytoplankton and clam (*Tapes philippinarum*) biomass in Barbamarco Lagoon, Italy. Estuar Coast Shelf Sci 79: 187–203

Thingstad TF, Zweifel UL, Rassoulzadegan F (1998) P limitation of heterotrophic bacteria and phytoplankton in the northwest Mediterranean. Limnol Oceanogr 43:88–94

Thingstad TF, Havskum H, Zweifel UL, Berdalet E and others (2007) Ability of a 'minimum' microbial food web model to reproduce response patterns observed in mesocosms manipulated with N and P, glucose, and Si. J Mar Syst 64:15–34

Trottet A, Roy S, Tamigneaux E, Lovejoy C, Tremblay R (2008) Impact of suspended mussels (*Mytilus edulis* L.) on plankton communities in a Magdalen Islands lagoon (Québec, Canada): a mesocosm approach. J Exp Mar Biol Ecol 365:103–115

Ulses C, Auger PA, Soetaert K, Marsaleix P and others (2016) Budget of organic carbon in the North-Western Mediterranean open sea over the period 2004–2008 using 3-D coupled physical-biogeochemical modeling. J Geophys Res Oceans 121:7026–7055

Vidussi F, Mostajir B, Fouilland E, Le Floc'h E and others (2011) Effects of experimental warming and increased ultraviolet B radiation on the Mediterranean plankton food web. Limnol Oceanogr 56:206–218

Wunsch C (1978) The North Atlantic general circulation west of 50°W determined by inverse methods. Rev Geophys 16:583–620

Zaldívar JM, Cattaneo E, Plus M, Murray CN, Giordani G, Viaroli P (2003) Long-term simulation of main biogeochemical events in a coastal lagoon: Sacca Di Goro (northern Adriatic Coast, Italy). Cont Shelf Res 23: 1847–1875

Appendix. Optimisation method

The ecosystem model was considered an application $M : \mathbb{R}^m \rightarrow \mathbb{R}^n$, where n is the number of experimental observations (here, n = 54) and m is the number of parameters (m = 166 in the model without oysters). With the application M being non-linear, the component $(p_i)_{1\leq i\leq m}$ of the control parameter vector P was optimised iteratively to reduce the gap between the observations, denoted $(d_j)_{1\leq j\leq n}$, and the corresponding simulation results, denoted $(c_j)_{1\leq j\leq n}$. The error associated with observation d_j was denoted r_j. In practice, in order to set the initial value of the cost function to 1 and give the same importance to each observation in the optimisation, r_j was chosen to be equal to the difference $(d_j - c_j)$ of the first iteration. This optimisation procedure finally consisted of minimising a quadratic cost criterion (Eq. A1):

$$F(P) = \sum_{j=1}^{n} \left(\frac{d_j - c_j}{r_j} \right)^2 \quad (A1)$$

The vector of parameters, P_0, was defined as the first guess of the iterative method and corresponded to the initial simulation. $P_k \in \mathbb{R}^m$ was then defined as the control parameter vector for iteration number k. The vector of the difference between observed and simulated results $(d_j - c_j)$ for iteration number k, denoted $P_k \in \mathbb{R}^n$, was introduced. To find the optimal parameters, the aim was to determine $\Delta P = P_{k+1} - P_k$, which solved Eq. (A2):

$$M'(P_k) \times \Delta P = R_k \quad (A2)$$

where $M'(P_k)$ is the tangent application of M evaluated at point P_k. $M'(P_k) = \left(\frac{\partial c_j}{\partial p_i} \right)_{1\leq i\leq m}^{1\leq j\leq n}$, with a dimension of n × m, is also called the Jacobian matrix of the system. This yields the system of unknowns Δp_i, with $1 \leq i \leq m$:

$$\sum_{i=1}^{m} \frac{\partial c_j}{\partial p_i} \times \Delta p_i = d_j - c_j, \text{ for } 1 \leq j \leq n \quad (A3)$$

Each component $\left(\frac{\partial c_j}{\partial p_i} \right)$ was approximated by $\left(\frac{\delta c_j}{\delta p_i} \right)$ after small explicit perturbations of each parameter δp_i and compilation of deviations of the model results δc_j. This step required running the model (m + 1) times at every iteration: a first simulation run without perturbation and then m simulation runs with only parameter m perturbed. For this reason, the optimisation method could have a high computational cost. However, in the present work, the duration of a simulation run was very short and was not limiting in the process.

The system must be dimensionless for both parameters and observations. To render the system dimensionless regarding parameters, a parameter weight diagonal matrix S, containing the *a priori* variances of the control parameters, was inserted (Eq. A4):

$$S_{i,j} = \sigma_i^2, \text{ for } 1 \leq i \leq m \quad (A4)$$

In the present study, S was practically chosen to reduce $S^{-\frac{1}{2}} \times P_0$ to the vector identity. A weight diagonal matrix W containing the *a priori* weight of each observation was also introduced to render the system dimensionless regarding observations (Eq. A5):

$$W_{j,j} = \frac{1}{r_j^2}, \text{ for } 1 \leq j \leq n \quad (A5)$$

W was assumed to be diagonal here, which meant that the observations were uncorrelated. The advantage of using these 2 matrices is the ability to choose a more or less important weight for a specific parameter or observation. Then, Eq. (A6) was obtained from Eq. (A2), introducing the new weight matrices:

$$W^{\frac{1}{2}} \times M'(P_k) \times S^{\frac{1}{2}} \times S^{-\frac{1}{2}} \times \Delta P = W^{\frac{1}{2}} \times R_k \quad (A6)$$

Eq. (A6) was an under-determined system A × Q = T, with a number of equations (n = 54) strictly smaller than the number of unknowns (m = 166). The matrix $A = W^{\frac{1}{2}} \times M'(P_k) \times S^{\frac{1}{2}}$ was thus singular, and various combinations of parameters resulted in the same simulation. Matrix A can be decomposed by singular value decomposition (SVD) as follows:

$$A = U \times L \times V^t \quad (A7)$$

where L is a diagonal matrix of eigenvalues, U is a base of eigenvectors in the space of data, and V is a base of eigenvectors of parameters. As A was singular, some of the singular values were zero and defined the null space of the system and thus the rank. In practice, due to numerical computation, those values were not strictly zero, and the rank was difficult to define. It was typically between 5 and 20. The collinearities between parameters led to a rank deficiency problem, and the pseudo-inverse was influenced by small eigenvalues. The system was then truncated at rank r using the sphericity test of Gonzalez Vicente (1986). Without this truncation, the new estimated parameters could be far from their starting point, which was not desirable in terms of keeping the model realistic. The solution was finally calculated using Eq. (A8):

$$\Delta P = S^{\frac{1}{2}} \times V_r \times L_r^{-1} \times U_r^t \times W^{\frac{1}{2}} \times R_k \quad (A8)$$

where V_r, L_r, and U_r were the truncated matrices associated with V, L and U, respectively.

The diagonal elements of matrix $(V_r \times V_r^t)$ were estimators of the determination of each control parameter and were called parameter resolutions. The matrix $(U_r \times U_r^t)$ gave similar information for the data, and its diagonal elements were called data resolutions. They showed the contribution of each observation as useful information to the system (e.g. Wunsch 1978).

Editorial responsibility: Stephen Wing, Dunedin, New Zealand

Submitted: October 18, 2019; Accepted: April 1, 2020
Proofs received from author(s): May 1, 2020